Palaeomagnetic Studies on Mafic Dykes
of the Shackleton Range, Antarctica,
and Their Geotectonic Relevance

By Rüdiger Hotten*

Summary: During the Geological Expedition to the Shackleton Range, Antarctica (GEISHA) in 1987/88, samples were taken from twenty-one basaltic dykes for palaeomagnetic investigations. The directions of characteristic remanent magnetization (ChRM) of the dykes were determined by thermal and alternating-field demagnetization of 268 cores drilled from the specimens collected. Moreover, on account of the hydrothermal and sometimes low-grade metamorphism of the dyke rock and the resulting partial modification of the primary magnetization, not only were comprehensive magnetic studies carried out, but also ore-microscopic examination. Only thus was it possible to achieve a reasonable assessment and interpretation of the remanent magnetization.

Jurassic and Silurian-Devonian ages were confirmed for the dykes of the northern and northwestern Shackleton Range by comparison of the paleopole positions calculated on the basis of the ChRM of the dykes with the known pole positions for the eastern Antarctic, as well as with polar-wandering curves for Gondwana. Radiometric ages were also determined for some of the dykes. Middle and Late Proterozoic ages are postulated for the dykes in the Read Mountains.

Conclusions on the geotectonic relations of the Shackleton Range can also be drawn from the palaeomagnetic data. It has been postulated that the main strike direction, which differs distinctly from that of the Ross orogen, is due to rotation or displacement of the Shackleton Range crustal block; however, this was not corroborated. The pole positions for the Shackleton Range agree with those of rocks of the same age from other areas of East Antarctica and its positions in the Palaeozoic-Mesozoic polar-wandering path for Gondwana are evidence against the idea of rotation and rather suggest that the position of the Shakleton Range crustal block is autochthonous.

Zusammenfassung: Während der „Geologischen Expedition in die Shackleton Range, Antarktika" (GEISHA) 1987/88 wurden 21 mafische Gänge basaltischer Zusammensetzung für paläomagnetische Untersuchungen beprobt.

Durch thermische und Wechselfeld-Entmagnetisierung von insgesamt 268 aus den Handstücken herausgebohrten Kernproben wurden die charakteristischen remanenten Magnetisierungsrichtungen (ChRM) der Gänge ermittelt. Darüber hinaus wurden aufgrund der hydrothermalen und z.T. niedrigmetamorphen Umwandlung des Gangmaterials und einer daraus resultierenden teilweisen Überprägung der primären Magnetisierung neben erzpetrographischen auch umfangreiche gesteinsmagnetische Untersuchungen durchgeführt. Erst dadurch war eine sinnvolle Bewertung und Interpretation der ermittelten Remanenzen möglich.

Durch einen Vergleich der aus den ChRM der Gänge errechneten Paläopolpositionen mit bekannten Polpositionen Ostantarktikas sowie mit Polwanderkurven Gondwanas konnten jurassische bzw. silurisch-devonische Alter der Dykes der nördlichen und nordwestlichen Shackleton Range, die an einigen der Gänge auch radiometrisch ermittelt wurden, bestätigt werden. Für die Gänge der Read Mountains sind dagegen mittel- und jungproterozoische Alter anzunehmen.

Die paläomagnetischen Daten lassen weiterhin Rückschlüsse auf die geotektonische Stellung der Shackleton Range zu. Vermutungen, deren Hauptstreich-

richtung, die von derjenigen des Ross-Orogens deutlich abweicht, sei auf eine Rotation oder Verschiebung des Shackleton Range-Krustenblocks zurückzuführen, konnten nicht bestätigt werden. Sowohl die Übereinstimmung der Pollagen mit Polpositionen gleichaltriger Gesteine anderer Gebiete Ostantarktikas als auch deren Positionen in der paläozoisch-mesozoischen Polwanderkurve für den Gondwana-Kontinent sprechen gegen eine solche Rotation und für eine autochthone Position des Shackleton Range-Krustenblocks.

1. INTRODUCTION

The geotectonic history of the Shackleton Range is subject to debate. Sometimes, it is considered to be a branch of the Ross orogenic belt or an aulacogen; sometimes it is viewed as a crustal fragment that rotated to its present position or as an „allochtonous terrane". The paleomagnetic studies of mafic dykes described below may help - by comparison with paleomagnetic studies of other regions - to clarify whether the Shackleton Range drifted a large distance as a crustal fragment and whether it was rotated.

In the Shackleton Range (20 °W to 31 °W, and 80 °S to 81 °S), hypabyssal basaltic dykes cut the crystalline basement and sometimes the overlying sediments discordantly (Fig. 1). SPAETH et al. (1995) provide detailed information on type and frequency of these intrusions (referred to in this paper as mafic dykes), on their mode of occurrence, petrography, geochemistry and radiometric ages.

It is therefore not necessary to give a description of the dykes and the reader is referred to the above paper. The numbering of the dykes used in the paper by SPAETH et al. (1995) is also used in this paper (nos. 1-14 for the dykes of the Read Mountains, southern Shackleton Range, and nos. 15-28 for those of the Haskard Highlands, Lagrange Nunataks and Herbert Mountains, northwestern and northern Shackleton Range, see Fig. 1); similarly, the dykes are subdivided by SPAETH et al. (1995) according to their petrography, geochemistry, and isotope geochemistry into the following dyke groups or generations (see Tabs. 1, 2, and 3):

Groups I, II and III belong to northern and northwestern Shackleton Range and are slightly (Group I) to intensely (Group III) hydrothermally altered);

Groups IV and V belong to the Read Mountains and are intensely hydrothermally altered and also slightly regionally metamorphosed.

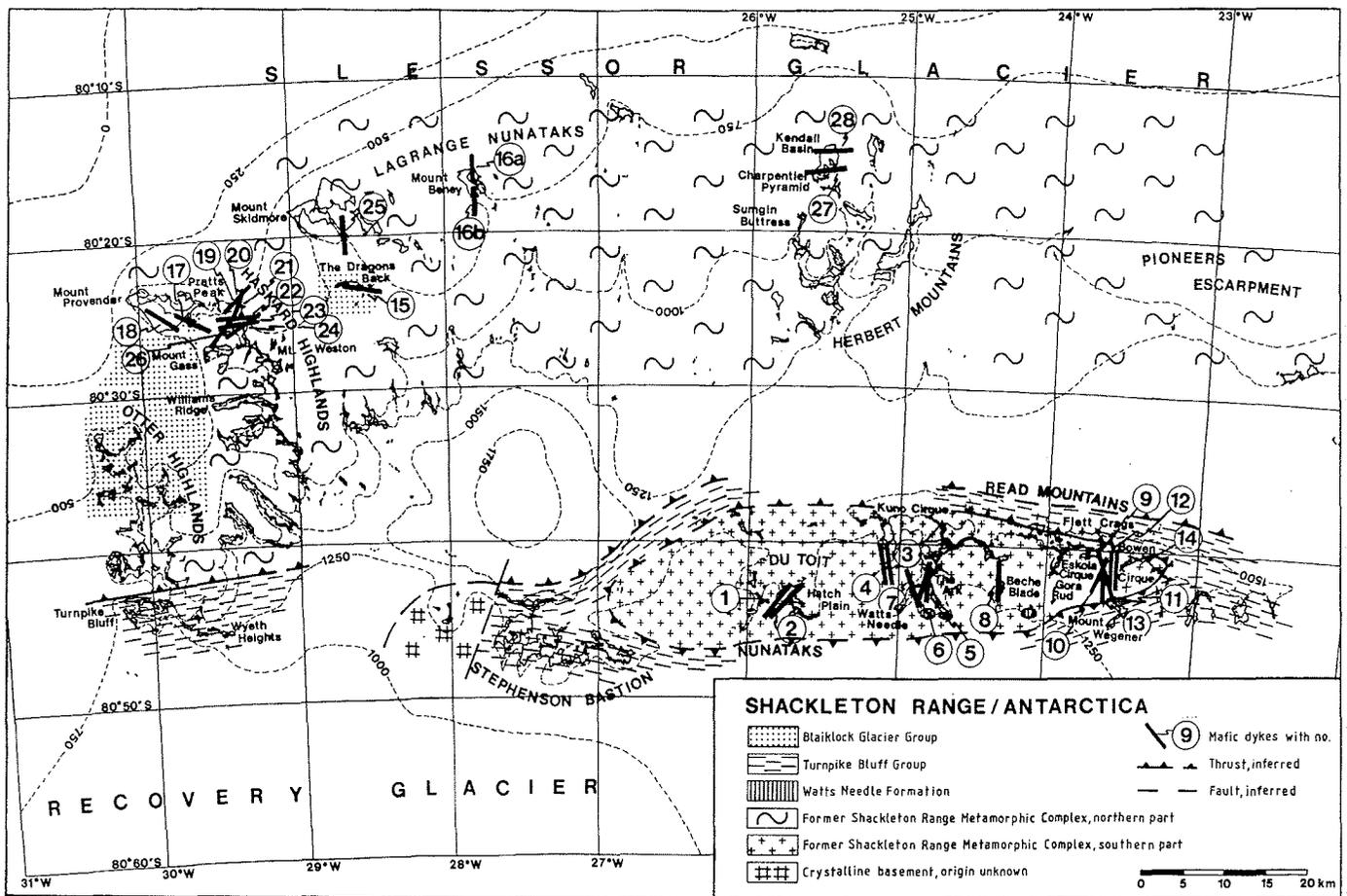* Dr. Rüdiger Hotten, Gadumer Straße16, D-59425 Unna, Germany.

Fig. 1: Geological map of the Shackleton Range and position of the mafic dykes (topography after the 1: 250,000 topographical map of the Shackleton Range of the British Antarctic Survey, 1980; geology modified after BUGGISCH et al. 1990).

Abb. 1: Geologische Karte der Shackleton Range und Lage der mafischen Gänge (Topographie nach der topographischen Karte der Shackleton Range 1: 250.000 des British Antarctic Survey, 1980. Geologie in Anlehnung an BUGGISCH et al. 1990).

Twenty-one mafic dykes were sampled for palaeomagnetic studies. The remaining dykes were not sampled for this purpose because of the poor state of preservation of the primary minerals, and in some cases because of their poor accessibility. The latter include the four dykes of basalt group III (see SPAETH et al. 1995). Altogether 94 oriented samples of unweathered rock weighing several kg each were collected from the dykes of the other groups, i.e. I, II, IV, and V, (depending on the thickness of the dyke, three to seven rock samples per dyke over the entire width of the outcrop). Altogether, 268 cores were drilled from this material.

The magnetic and palaeomagnetic analysis of these samples was carried out at the Institute for Geophysics, University of Münster. The sampling procedure, the methods used for investigating the samples and the results obtained are described in detail in HOTTEN (1993).

2. MAGNETIC STUDIES

The primary magnetization of these rocks has been partially modified as a result of hydrothermal alteration and in some ca-

ses low-grade metamorphism. Therefore, magnetic analyses in the laboratory are of particular importance to the understanding and interpretation of the results of the palaeomagnetic studies.

Together with the results of ore microscopy summarized in Tab. 1, the magnetic analyses are used for interpretating the remanence values determined by alternating-field and thermal demagnetization. After the demagnetization tests had been completed, one to three cores (depending on the demagnetization behaviour of the material) were selected from each dyke; they were thermomagnetically analyzed and hysteresis loops were plotted.

2.1 Thermomagnetic analysis

In almost all polished sections, ore-microscopic analysis (see Tabs. 1-4) showed high-temperature oxidation, stages 2 to 3 at a maximum (after WILSON & WATKINS 1967, ADE-HALL et al. 1968, see Table 1), evidenced by the occurrence of ilmenite exsolution lamellae. Low-temperature oxidation of the titanomagnetites was found to display a broader range (maghemitization, stages 1 to 4; after JOHNSON & HALL 1978), and hydrothermal alteration of the minerals, i.e. the younger basalts (Me-

124

Dyke	d_{max} (mm)	vol.%	HTO	LTO	hydrothermal alteration	ore minerals
Group I						
16a	0.15	4.2	2-3	1-2	x	(m)TiMa, ilmenite, pyrite
16b	0.3	9.3	3	1-2	x	(m)TiMa, ilmenite, pyrite, Ti hematite
25	<0.01	17.4	1-2	1-2	xxx	mTiMa, TiMa, ilmenite, pyrite, Ti hematite
Group II						
15	0.4	11.7	2	3	x	mTiMa, TiMa, ilmenite, Ti hematite, sphalerite
19	0.3	18.0	2	1	xx	TiMa, pyrite, ilmenite, chalcopyrite, sphalerite, hemati-te
21	0.15	14.4	3	2	xx	(m(TiMa, ilmenite, pyrite, chalcopyrite
23	0.15	10.7	2-3	2-3	xxx	mTiMa, ilmenite, pyrite, sphalerite
24	0.3	12.9	2-3	2	xx	(m)TiMa, ilmenite, pyrite, Ti hematite
27	0.4	11.9	3	3	xxx	mTiMa, TiMa, ilmenite, pyrite, sphalerite, hematite
Group IV						
1	0.8	4.9	2-3	3	xxx	mTiMa, TiMa, ilmenite, pyrite, Ti hematite
2	0.7	3.1	2-3	?	xxxxx	TiMa completely altered, ilmenite, pyrite, Ti hematite
7	0.5	4.6	2-3	?	xxxxx	TiMa completely altered, partly rimmed by magnetite, ilmenite, Ti hematite
8	03	8.5	1	3-4	xxxx	mTiMa, ilmenite, pyrite
9	1.0	6.2	2-3	?	xxxxx	TiMa much altered, partly rimmed by magnetite, ilmenite pyrite, Ti hematite
11	0.4	4.1	2-3	?	xxxxx	TiMa completely altered, ilmenite, pyrite
12	0.3	1.2	?	?	xxxxx	TiMa completely altered, but rarely recroystallized grains, ilmenite, pyrite
13	1.4	7.0	2-3	3-4	xxx	mTiMa, TiMa, ilmenite, pyrite Ti hematite
GroupV						
5	2.0	11.6	2-3	3-4	xxxxx	mTiMa, TiMa, ilmenite, pyrite, Ti hematite, hematite
6	0.8	8.9	2-3	?	xxxxx	TiMa completely altered, some fine-grained relics or new grains, ilmenite, pyrite, Ti hematite

Tab. 1: Results of ore-microscopic studies. d_{max} = maximum grain size; vol.% = percentage of total mineral content; HTO and LTO = class of high- or low-temperature oxidation, respectively; (m)TiMa / mTiMa = very slightly maghemitized titanomagnetite; mTiMa = maghemitized titanomagnetite; x,xx,xxx,... = relative degree of hydrothermal alteration.

Tab. 1: Ergebnisse der erzmikroskopischen Untersuchungen. d_{max} = maximale Korngröße, vol.% = prozentualer Anteil am Gesamtmineralbestand, HTO und LTO = Klasse der Hoch- bzw. Tieftemperaturoxidation, (m)TiMa / mTiMa = sehr gering maghemitisierter zu maghemitisiertem Titanomagnetit; x, xx, xxx, ... = zunehmende Intensität hydrothermaler Mineralumwandlungen.

sozoic) are less altered, and the (Palaeozoic?) basalts of the northern Shackleton Range and the (Proterozoic?) basalts of the Read Mountains (Fig. 2-5) more altered; some of the latter have undergone low-grade metamorphism. In subaerial basalts, low-temperature oxidation often grades into hydrothermal alteration (PETERSEN 1982). The effects of these two processes cannot normally be distinguished under the microscope or by magnetic methods. These transformation processes are important because they change the magnetic properties of the rock. They cause, for example, the Curie temperature to increase to a maximum of 680 °C (PETERSEN 1982). High-temperature oxidation, which in the case of igneous rocks must be interpreted as synmagmatic, causes ilmenite lamellae to form by exsolution, thus decreasing the effective grain size, which increases the stability of the primary thermoremanent magnetization (TRM). Low-temperature oxidation or hydrothermal alteration, however, may be the consequence of autohydrothermal or postmagmatic processes, e.g. regional metamorphism. As they cannot be assigned to a definite period of time, it must be checked whether they led to a chemoremanent magnetization (CRM) or not. As with thermoremanent magnetization caused by reheating, chemoremanent magnetization may completely alter the primary thermoremanent magnetization generated during cooling of the melt.

When the minerals in a rock have been affected by oxidation or hydrothermal alteration, this is reflected in the shapes of the thermomagnetic heating and cooling curves. The results of the measurements described below, during which the samples were not placed in an inert gas or in a vacuum, are readily correlatable with the information obtained by ore microscopy. Moreover, the magnetic properties are partially determined by minute
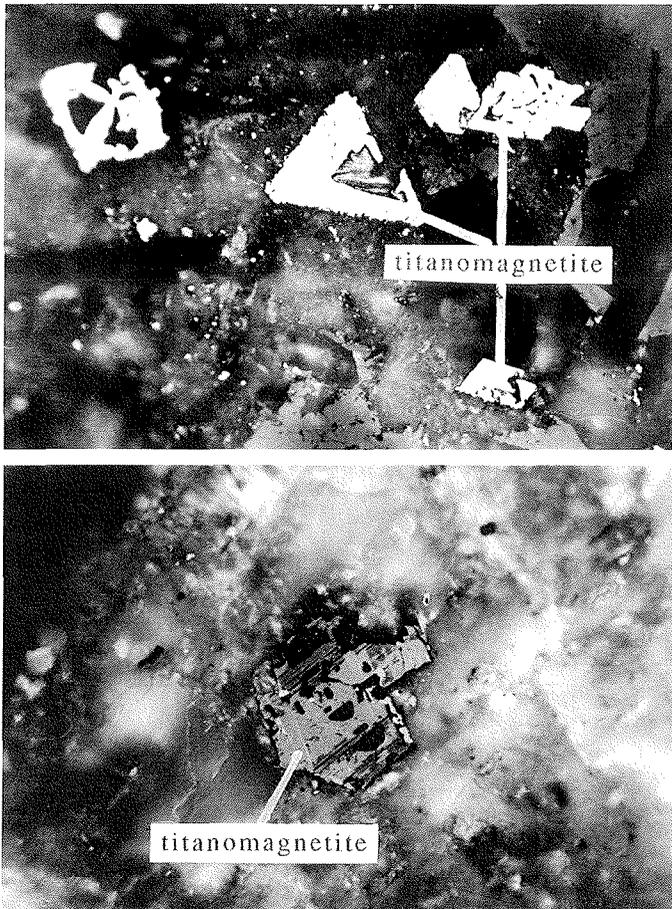
Fig. 2: a) Idiomorphic to hypidiomorphic titanomagnetite in a basalt sample of group I; occasional contraction cracks indicate initial maghemitization; plane-polarized light, lower margin = 0.53 mm. b) Anisotropic titanomagnetite of the high-temperature oxidation classes 2 and 3 in a basalt sample of Group I; crossed nicols, lower margin = 0.53 mm.

Abb. 2: a) Idiomorpher bis hypidiomorpher Titanomagnetit einer Basaltprobe der Gruppe I. Vereinzelte Schrumpfungsrisse weisen auf beginnende Maghemitisierung. Nicols parallel, unterer Bildrand = 0,53 mm. b) Anisotrop gefelderter Titanomagnetit der Hochtemperatur-Oxidationsklasse 2-3 einer Basaltprobe der Gruppe I. Nicols gekreuzt, unterer Bildrand = 0,53 mm.
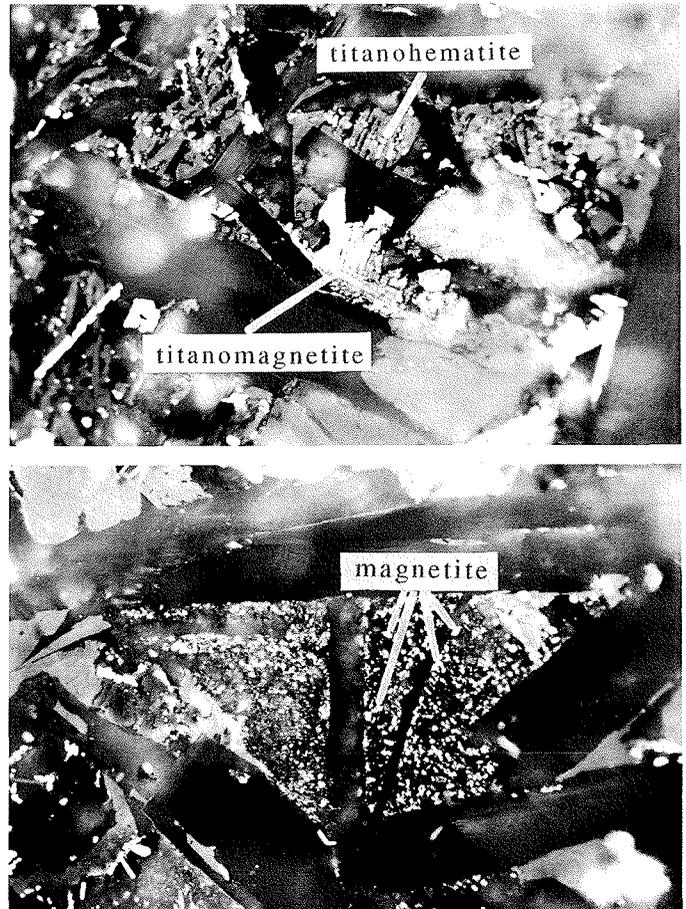
Fig. 3: a) Titanomagnetite hydrothermally altered to a granular aggregate (center) with occasional titanohematite in a sample of Group II; plane polarized light, lower margin = 0.53 mm. b) Fine-grained magnetite (center) in hydrothermally competely altered pyroxene in a sample from dyke 25; plane polarized light, lower margin = 0.53 mm.

Abb. 3: a) Hydrothermal granulierter Titanomagnetit (Bildmitte) mit vereinzelter Neubildung von Titanohamatit einer Probe der Gruppe II. Nicols parallel, unterer Bildrand = 0,53 mm. b) Feinkörniger Magnetit in vollständig hydrothermal zersetztem Pyroxen (Bildmitte) einer Probe aus Dyke 25. Nicols parallel, unterer Bildrand = 0,53 mm.

magnetic minerals which are not recognizable under the microscope; thus, they provide additional information which is difficult to obtain otherwise. However, the complexity of the possible mineral transformations and formation of new minerals that take place during heating in the laboratory depend both on the mineralogical composition of the rock and on the chemical composition of the various minerals, as well as on the maximum temperature reached, often leads to ambiguity in interpreting the curves.

Many similar thermomagnetic curves were obtained. Comparable curves were used to set up standard types of curve (Figs. 6 and 7). In principal, two types of curve were distinguished. Type I curves indicate a higher saturation magnetization before heating than after cooling (M_S/M_S' ratio >1). Type II curves show a higher saturation magnetization after cooling than before heating ($M_S/M_S' <1$). These two types of curve can be further subdivided on the basis of differing M/M' ratios and the

Curie temperatures obtained during heating (T_C) and cooling (T_C'). However, in all cases the heating process was associated with a decrease of the maximum Curie temperature.

Tab. 2 gives a list of the data obtained. Assessment of the effects of oxidative or hydrothermal processes was based on comparison with thermomagnetic curves taken from the literature listed in the table. Sometimes, the results differ from those derived from ore microscopic analysis (see Tab. 1); these differences can be explained by the fact that either alteration has more effect on submicroscopic mineral grains or, for example, that very fine-grained magnetite crystals are often included in other minerals (biotite, pyroxene) and are thus better protected against alteration.
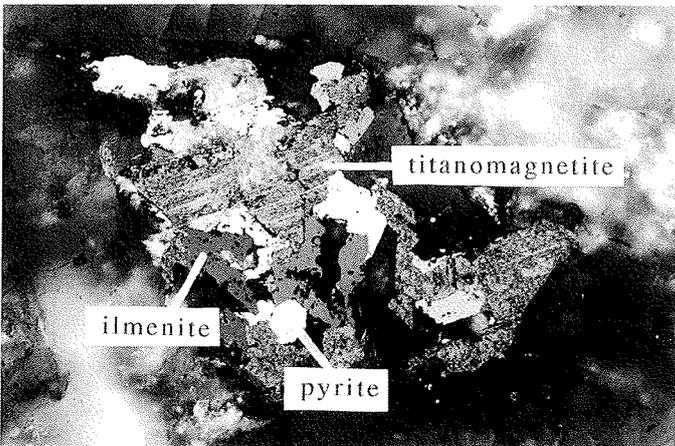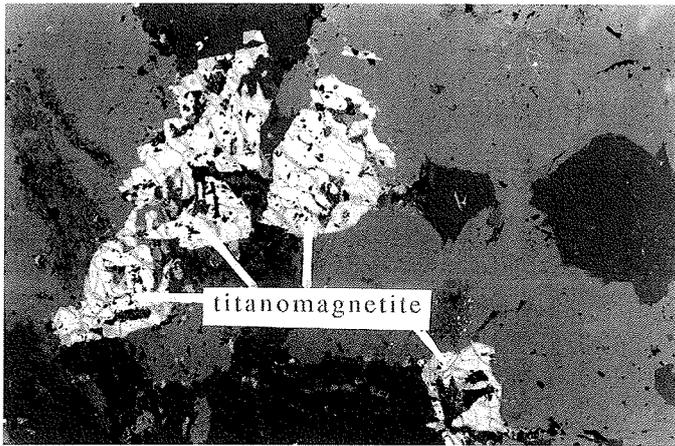
Fig. 4: a) Contraction cracks in titanomagnetites widened by progressive maghemitization (light grains) in a sample of Group IV; plane polarized light, lower margin = 0.87 mm. b) Pyrite (white grains), ilmenite (dark-grey grains) and exsolved (HTO 2-3) titanomagnetite hydrothermally altered to a granular aggregate (grey grains) in a sample of Group IV; crossed nicols, lower margin = 0.87 mm.

Abb. 4: a) Durch fortgeschrittene Maghemitisierung aufgeweitete Schrumpfungsrisse in Titanomagnetiten (helle Körner) einer Probe der Gruppe IV. Nicols parallel, unterer Bildrand = 0,87 mm. b) Pyrit (weiße Körner), Ilmenit (dunkelgraue Körner) und entmischter (HTO 2-3), durch hydrothermale Prozesse granulierter Titanomagnetit (mittelgraue Körner) in einer Probe der Gruppe IV. Nicols gekreuzt, unterer Bildrand = 0,87 mm.

Fig. 5: a) Titanomagnetite (center) of the HTO 2-3 and ilmenite (right) in a sample of Group V. Whereas the ilmenite is well preserved (exsolution lamellae and individual grains, e.g. upper margin), most of the exsolved magnetite has been hydrothermally altered to a granular aggregate or replaced by titanohematite; crossed nicols, lower margin = 0.87 mm. b) Former titanomagnetite and ilmenite in a sample of Group IV. Titanomanetite is nearly completely replaced by non-opaque minerals; crossed nicols, lower margin = 0.87 mm.

Abb. 5: a) Titanomagnetit (Bildmitte und rechts) der HTO 2-3 und Ilmenit in einer Probe der Gruppe V. Während Ilmenit (Entmischungslamellen und Einzelkörner, z.B. oberer Bildrand) gut erhalten ist, ist der entmischte Magnetit weitgehend hydrothermal granuliert oder durch Titanohämatit ersetzt. Nicols gekreuzt, unterer Bildrand = 0,87 mm. b) Ehemaliger Titanomagnetit und Ilmenit in einer Probe der Gruppe IV. Titanomagnetit ist nahezu vollständig durch nichtopake Minerale ersetzt. Nicols gekreuzt, unterer Bildrand = 0,87 mm.

TYPE I CURVES

Type I curves indicate the presence of magnetite that is mostly poor in Ti and/or exsolved and maghemitized magnetite or titanomaghemite, which on heating unmix to a non-magnetic or weakly magnetic mineral phase (hemo-ilmenite or hematite) and (Ti-)magnetite. After cooling, the saturation magnetization is weaker than before heating (BÖHNEl 1985).

Curve I.1 (see Fig. 6) shows an almost identical magnetization both before and after heating. The Curie temperatures during cooling are distinctly lower (519 and 540 °C, Tab. 2) than during heating (546 and 552 °C, Tab. 2). This behavior indicates that the magnetic mineral is possibly maghemitized titanomagnetite which is poor in titanium and unmixes to magnetite and hematite (BÖHNEL 1985).
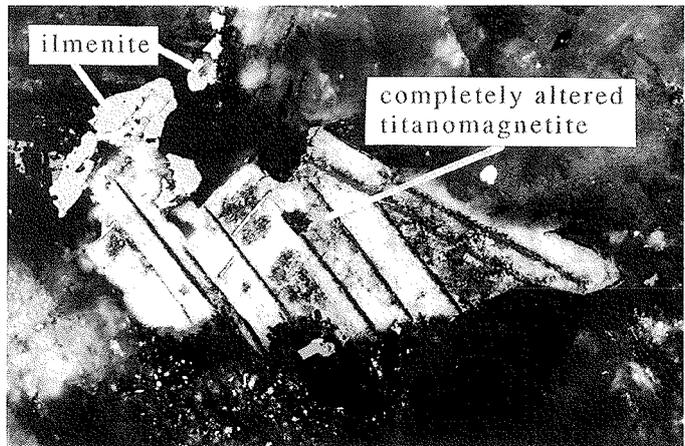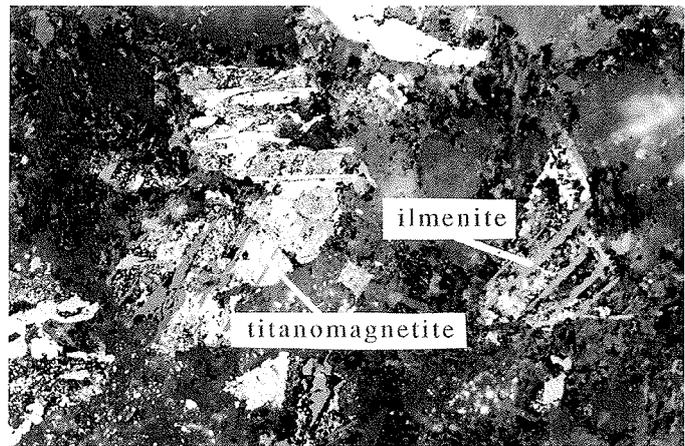
Curves of this type are obtained from samples from dyke 5. Microscopically, both under transmitted light and under reflected light, the rock shows distinct alteration and contains secondary minerals (Tab. 1, HOTTEN 1993, SPAETH et al., 1995), amongst which various generations of ore minerals can be distinguished. The primary mineral is partly granular titanomagnetite containing exsolved ilmenite which was oxidized at low temperatures and hydrothermally altered (Figs. 4 and 5). Moreover, very fine-grained magnetite, pyrite, and hematite, most probably secondary minerals, are found within chloritized and/or serpentized augite grains. The type of curve obtained from these secondary magnetites indicates that they are the true carriers of the magnetization, whereas the primary ferrimagnetic minerals have been so altered and replaced by paramagnetic minerals that they are hardly reflected in the curve. The samples of other Read

Dyke No.	Sample	Type	T_{C1} (°C)	T_{C2} (°C)	$T_{C'}$ (°C)	HTO (1)	hydrothermal alteration (1) (2)	Magnetization carrier (1) (2) (3)
Group I								
16a	XIV 2A	1.2	300	572	497	2-3	(x)	TiMagh or TiMa
16b	XIX 2B	1.2	279	567	432	1-2	(x)	TiMagh or TiMa
	XIX 4.1 B	1.2	259	573	548	2	(x)	TiMagh or TiMa
25	XX 3B	11.4	287	572	527	2	xxxx	mTiMa
	XX 5.2B	11.4	287	527	522	2	xxxx	mTiMa
Group II								
15	XIII 3.1A	1.2	409	587	527	2	x	TiMagh or TiMa
19	XV 1.1A	11.2	-	572	517	3-4	xx	TiMagh
21	XVI 3.2B	11.2	-	586	522	3-4	xx	TiMagh
	XVI 5B	11.2	-	586	544	3-4	xx	TiMagh
23	XVII 1B	11.2	-	577	546	3-4	xx	TiMagh
	XVII 3.2B	11.2	-	575	542	3-4	xx	TiMagh
	XVII 4B	11.2	-	572	557	3-4	xx	TiMagh
24	XVIII 2.2A	11.2	-	577	547	3-4	xx	TiMagh
	XVIII 3A	11.2	-	572	531	3-4	xx	TiMagh
27	XXI 5.1A	1.3	456	606	586	3-4	xx	TiMagh or TiMa, Hem
Group IV								
1	I 1A	II.2	-	549	532	3-4	xx	TiMagh
	I 5.1A	II.1	-	550	525	1(sec)	xxxxxx	mTiMa
2	II 3A	II.3	314	552	539	2-3	xxx	mTiMa
7	VII 2.2B	II.3	330	577	539	2-3	xxx	mTiMa
	VII 4.1B	II.5	-	565	500	?	xxxxx	mTiMa
8	VIII 1B	II.1	-	550	522	1(sec)	xxxxxx	mTiMa
	VIII 2B	II.1	-	554	517	1(sec)	xxxxxx	mTiMa
9	IX 1.1B	II.3	314	562	524	2-3	xxx	mTiMa
	IX 4.2A	II.3	320	577	527	2-3	xxx	mTiMa
11	X 1.1B	II.5	-	557	512	4	xxxxx	mTiMa
	X 3A	II.6	-	557	532	4	xxxxxx	mTiMa
12	XI 1A	II.5	-	572	502	4	xxxxx	mTiMa
13	XII 1.1A	II.1	-	555	537	1(sec)	xxxxxx	mTiMa
	XII 4.1A	II.6	-	555	537	4	xxxxxx	mTiMa
Group V								
5	V 2.1A	I.1	-	546	519	1(sec)	xxxxxx	mTiMa
	V 3.1A	I.6	-	552	540	1(sec)	xxxxxx	mTiMa
6	VI 2A	II.6	-	567	530	3-4	xxxxx	mTiMa

Tab. 2: Thermomagnetic data. mTiMa = maghemitized titanomagnetite; TiMagh = titanomaghemite; Häm = hematite; T_C = Curie temperatures; HTO = high-temperature oxidation; x,xx,xxx,... = degree of hydrothermal alteration; sec = secondary. (1) see ADE-HALL et al. (1971); (2) see LØVLIE (1987), (3)see WORM (1981) and BÖHNEL (1985).

Tab. 2: Ergebnisse der thermomagnetischen Messungen. mTiMa = maghemitisierter Titanomagnetit, TiMagh = Titanomaghemit, Häm = Hämatit, T_C = Curie-Temperatur, HTO = Hochtemperaturoxidation; x, xx, xxx, ... = zunehmende Intensität hydrothermaler Mineralumwandlungen, sec = sekundär. (1) nach ADE-HALL et al. (1971); (2) nach LØVLIE (1987), (3) nach WORM (1981), BÖHNEL (1985)

Mountains dykes which underwent similar secondary alteration, but in which relict primary titanomagnetite is present, give a completely different curve (see below). In the case of type I.1 curves, the characteristic remanent magnetization (ChRM) obtained by step demagnetization is probably derived from a late, secondary CRM but not from the primary TRM.

Type I.2 curves (Fig. 6) show a distinctly lower M_S'. They are characteristic of the fresh (Mesozoic) dykes 16a and 16b, and also the hydrothermally altered (Palaeozoic) dyke 15. In the heating curve, two Curie temperatures can be recognized. The lower temperature (T_{C1}), which is rather weak, ranges between 260 and 300 °C and corresponds to the almost unaltered material. The other Curie temperature of 409 °C corresponds to hy-

drothermally altered material. T_{C2} ranges between 567 and 587 °C. T_C' is generally between 497 and 548 °C.

Curves of this type are formed when titanomaghemite is transformed to titanomagnetite or titanohematite on heating (WORM 1981, BÖHNEL 1985). In the first case, the oxygen anions released are fixed by reducing gases resulting in further reduction of the amount of Fe-Ti oxides present. This in turn leads to formation of a stoichiometric titanomagnetite, the Fe/Ti ratio of which equals that of the material before heating. Its Curie temperature is lower (WORM 1981). According to PRICE (1980), it is possible that exsolution of titanomagnetite similar to that caused by high-temperature oxidation took place; in this case, it is probably submicroscopic. The iron-rich zones have a higher Curie temperature than the original material, whereas that of the titanium-rich lamellae lies below room temperature. This kind of intimate exsolution may be reversed above 600 °C, since the titanomagnetites form a continuous solid-solution series at high temperatures.

As with T_{C1} and T_{C2}, titanomaghemites and titanomagnetites with two different compositions (i.e. different titanium contents) carry the magnetization. Heating curves of this kind (I.2, Fig. 6) are characteristic of material that has undergone high-temperature oxidation, i.e. stage 2 (ADE-HALL et al. 1971) and that shows slight hydrothermal alteration or none at all. „Internal oxidation" without access to atmospheric oxygen is typical of subaerial basalts and gabbros. Titanomagnetite is oxidized owing to internal buffering of the rock complex, which cools as a more or less closed system. On cooling, the original Fe-Ti oxides form intergrowths of ilmenite and magnetite. Titanomagnetites which crystallize from the silicate melt and have not undergone „internal oxidation" and/or exsolution show Curie temperatures between 244 and -41 °C (0.5 < x < 0.85). The process described here increases the Curie temperature to 580 °C (HARGRAVES & PETERSEN 1971).

Additional electron probe studies on magmatic titanomagnetites that are clearly identifiable as primary yielded TiO_2 contents between 11 and 28 wt.%; most of the fine-grained, non-oxidized, possibly secondary magnetites are below 1 wt. % TiO_2. The variable Curie temperatures are possibly due to several generations of magnetite of differing composition.

Curve type I.3 (dyke 27) shows a similar shape; the difference between M_S and M_S', however, is much greater. Differences were also found in the Curie temperatures. T_{C1} is distinct at 456 °C. The induced magnetization, however, is still high at this temperature. A further increase in temperature is accompanied by a further linear decrease of the magnetization; another Curie temperature (T_{C2}) occurs at 606 °C, but is faint. This second Curie temperature indicates that, in addition to titanomaghemite or titanomagnetite, a considerable amount of hematite is also present. This is confirmed by ore-microscopic examination of the same core, which in fact yielded a high percentage of hematite and altogether displays somewhat more intense hydrothermal alteration than the cores of curve type I.2. The reduction of grain size caused by this alteration probably made the

grains more susceptible to changes in magnetization during heating and thus intensified those alteration processes which lead to a reduction of the saturation magnetization on cooling. Studies by ADE-HALL et al. (1971) on rocks showing intense hydrothermal alteration yielded similar curves.
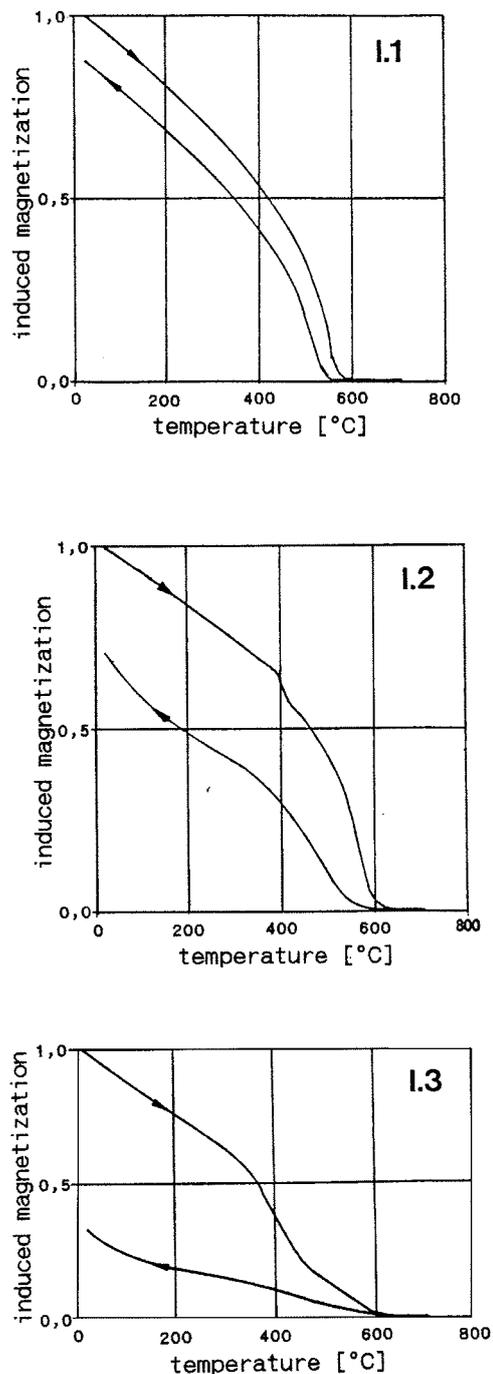

Fig. 6: Representative thermomagnetic curves of the Shackleton Range samples, normalized with respect to the maximum magnetization. Heating and cooling were done in air. Before heating of the samples, the induced saturation magnetization (M_S) is higher than after cooling (M_S').

Abb. 6: Typisierte thermomagnetische Kurven der Shackleton-Range-Proben, normiert auf die größte jeweils auftretende Magnetisierung. Aufheizung und Abkühlung in Luft. Vor dem Aufheizen der Proben ist die induzierte Sättigungsmagnetisierung höher als nach dem Abkühlen.

TYPE II CURVES

Type II curves show a higher saturation magnetization after cooling than before heating (see Fig. 7).

Type II.1 curve is similar in shape to curve I.1. Here, too, the similarity of the two curves at almost the same Curie temperatures (T_C: 550-555 °C, T_C': 517-537 °C) suggests that a Ti-poor maghemitized titanomagnetite is the carrier of the magnetization; during heating, it exsolves into magnetite and hematite (BÖHNEL 1985, see above). After cooling, however, a slightly higher M' value is found, which is possibly due to neoformation of magnetite from non-opaque Fe-bearing minerals at temperatures of >600 °C (LØVLIE 1987). Curves of this shape are produced by cores from dykes 1, 8, and 13, which, like those from dyke 5 (type I.1), were taken from dykes in the Read Mountains that have undergone hydrothermal alteration or low-grade metamorphism (HOTTEN 1993, SPAETH et al. 1995). Microscopic analysis of these samples also yielded titanomagnetites or magnetites of two different generations. These comprise primary, partly granular, fine- to medium-grained idiomorphic grains (Figs. 4 and 5) which

have undergone high- and low-temperature oxidation and hydrothermal alteration, and secondly, fine-grained, xenomorphic, unaltered magnetites or narrow secondary rims of magnetite, so that here too a secondary CRM must be postulated, which is possibly superimposed on the primary TRM.

Type II.2 curves are typical of hydrothermally altered dykes in the northern part of the Shackleton Range, e.g. dykes 19, 21, 23, and 24. Only one core from dyke 1 (Read Mountains) shows the same behaviour. In all cases, distinct Curie temperatures were observed during the heating phase (T_C: 572-586 °C, dyke 1: 549 °C) and cooling phase (T_C': 517-557 °C, dyke 1: 532 °C). According to DOELL & COX (1965), the original mineral is postulated to be titanomaghemite, which exsolved into titanohematite and titanomagnetite; the titanomagnetite has a lower Curie temperature, but a higher saturation magnetization than the original titanomaghemite. It is possible, however, that here too the higher saturation magnetization after cooling is due to newly formed magnetite.

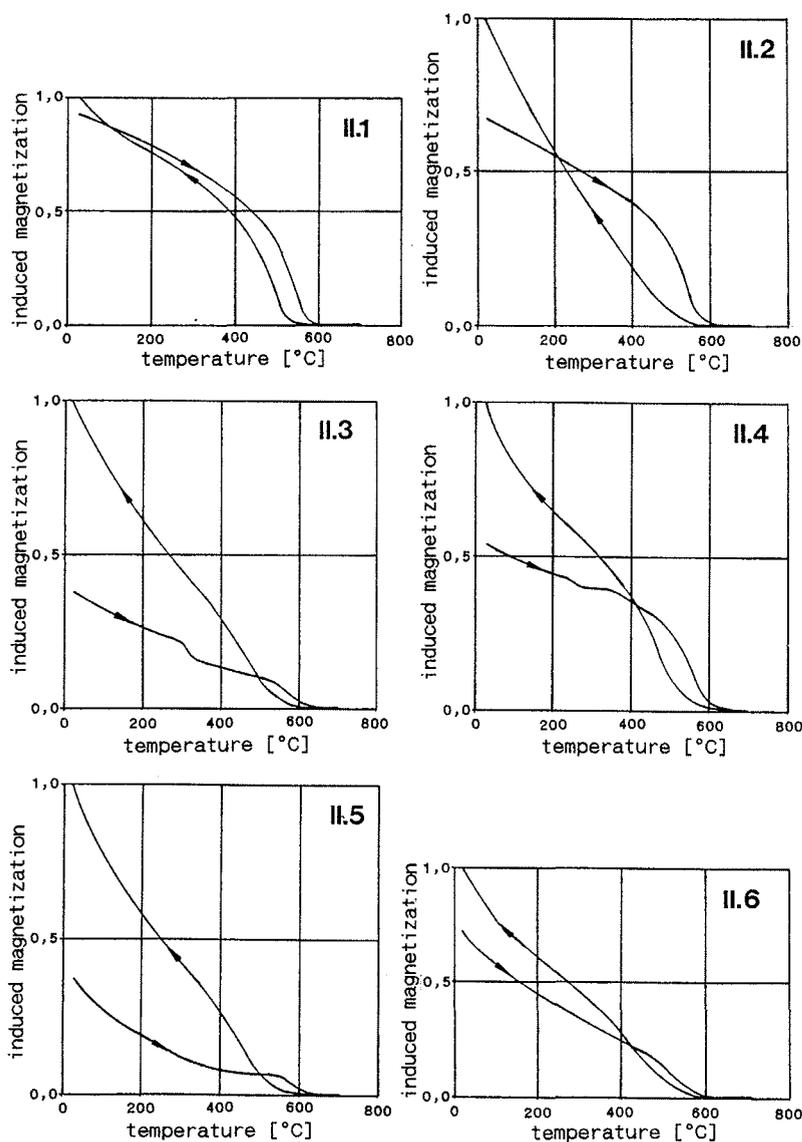The curves of types II.3, II.4, II.5, and II.6 are comparable to

Fig. 7: Representative thermomagnetic curves of the Shackleton Range samples, normalized with respect to the maximum magnetization. Heating and cooling were done in air. Before heating of the samples, the induced saturation magnetization (M_S) is lower than after cooling (M_S').

Abb. 7: Typisierte thermomagnetische Kurven der Shackleton-Range-Proben, normiert auf die größte jeweils auftretende Magnetisierung. Aufheizung und Abkühlung in Luft. Vor dem Aufheizen der Probe ist die induzierte Sättigungsmagnetisierung geringer als nach dem Abkühlen.

those described by LøVLIE (1987) for titanomagnetite-bearing rock belonging to high-temperature oxidation Classes 2 to 3, and showing considerable hydrothermal alteration of the opaque minerals. The difference between M and M', which is initially very large, becomes smaller with increasing alteration. The high values of M' may partly be due to alteration of titanomaghemite. LøVLIE (1987) infers a second generation of magnetite forms from non-opaque, Fe-bearing minerals, which causes an increase of the saturation magnetization.

Evidence for this kind of relationship has also been found in the author's cores. A core from dyke 6, for example, shows a distinctly higher degree of alteration than one from dyke 2 (see Tab. 2). Accordingly, dyke 6 gives a thermomagnetic curve of type II.6, and dyke 2 a curve of type II.3. However, sometimes various cores taken from one dyke show different degrees of hydrothermal alteration and correspondingly different types of curves (e.g. dyke 7, see also Tab. 2).

Measurements on cores from dykes 2, 7, and 9 yielded type II.3 curves, and from dyke 25 type II.4 curves. Both types of curves display the same two Curie points during the heating phase (T_{C1}: 287-330 °C; T_{C2}: 527-577 °C) and a Curie point at $T_C' < T_{C2}$ (T_C': 522-539 °C) during cooling. These temperatures may indicate the presence of Fe-Ti minerals with lower or higher Ti content or the presence of minerals with varying degrees of maghemitization, which in turn is probably due to variable grain size (WORM 1981). T_{C1} is less distinct in curve II.4 than in curve II.3. Curie points around 320 °C as documented in type II.3 curves may also be due to the presence of pyrrhotite. However, no pyrrhotite was found under the microscope.

In contrast to this, type II.5 and II.6 curves show only one T_C. Curie points at 555 to 572 °C indicate the presence of titanomagnetite poor in Ti or maghemitized titanomagnetite as carriers of the magnetization. Titanomagnetites with a lower T_C' of 500 to 537 °C (see above) are generated by exsolution or neoformation. Curves of type II.5 were obtained from cores from dykes 7, 11, and 12, and type II.6 to samples from dykes 6, 11, and 13. Titanomagnetite grains were observed to have partially exsolved ilmenite; the magnetite between the ilmenite lamellae had completely disappeared due to hydrothermal alteration and was no longer identifiable under the microscope (e.g. in samples from dyke 11).

2.2 Hysteresis loops

Other magnetic parameters were obtained from hysteresis loops and by generating IRM curves (see Tab. 3). Tab. 3 also shows a modified Königsberger-Q_{mod} ratio (STACEY & BANERJEE 1974), which allows the magnetic stability to be estimated. The intensity of the magnetic field of the earth, which is unknown for the time when the remanent magnetization was acquired, is neglected during calculation of the remanent magnetization.

Typical examples of IRM curves are shown in Fig. 8. Fig. 9 shows parts of hysteresis loops obtained with the vibrating sample magnetometer (VSM).

Here too, as in the thermomagnetic curves, various types of loops were obtained: a, b, c, and d (Figs. 8 and 9). Curves of types a and b which show high values for the remanent (Fig. 8) and induced (Fig. 9) saturation magnetization, but low coercivity are typical of samples containing titanomagnetite. The higher the proportion of particles with a single domain, the more stable the remanent magnetization and the stronger the coercivity at a consistently high saturation magnetization (THOMPSON & OLDFIELD 1986). On the other hand, an increase in maghemitization leads to a decrease in the coercivity. Probably for this reason, the cores from the Read Mountains dykes that showed more intense low-temperature oxidation must be assigned to type a (lower coercivity), and those from the dykes of the northern and northwestern parts of the Shackleton Range belong to type b (higher coercivity).

Hysteresis curves of type c with comparably low values of saturation magnetization and remanent saturation magnetization, but high coercivity indicate that hematite is the carrier of the magnetization.

Saturation magnetization was not reached in any of the examples shown in Fig. 9 (in particular Figs. 9b and c), but the hysteresis curve increases linearly with stronger magnetic fields. This increase is due to the paramagnetic susceptibility of the silicate groundmass. The saturation magnetization M_S, which is caused by the ferrimagnetic or antiferromagnetic mineral components, is obtained by extending the straight part of the curve until it intersects the ordinate (SCHMIDBAUER 1975).

Fig. 9d shows the hysteresis loop of a core with a low content of ferrimagnetic or antiferromagnetic minerals; correspondingly low saturation remanence values were obtained (see Fig. 8d). The shape of the loop is mainly determined by the paramagnetic component. Determination of the magnetization parameters from this kind of hysteresis loop proved to be very inaccurate. The M_{RS}/M_S and H_{CR}/H_C ratios were therefore not determined here (Table 3).

The majority of the analyzed cores can be assigned to curve types a and b; this confirms that titanomagnetite with variable grain sizes is the dominant carrier of the remanent magnetization. Correspondingly, the $H_{CR'}/H_{CR}$ ratio is between 1.3 and 1.5 (see Tab. 3), values around 1.5 indicating a magnetite very poor in titanium. The saturation remanences M_{RS} generally amount to several hundred A/m to more than a thousand A/m, and the coercivities of the remanent magnetization H_{CR} mostly show values between about 18 and 68 kA/m (Tab. 3).

The cores from dyke 25 in particular show indications of the presence of hematite (curve type c). $H_{CR'}/H_{CR}$ amounts to a little over 1.0 with comparatively low M_{RS} of 255 and 282 A/m, but very high of 136 and 146 kA/m, respectively.

Only few cores from the thermally metamorphosed dykes in the Read Mountains (7, 9, 11, and 12) show a predominantly paramagnetic behaviour of type d. The $H_{CR'}/H_{CR}$ ratio is sometimes around 1.0 and indicates the presence of hematite here too.
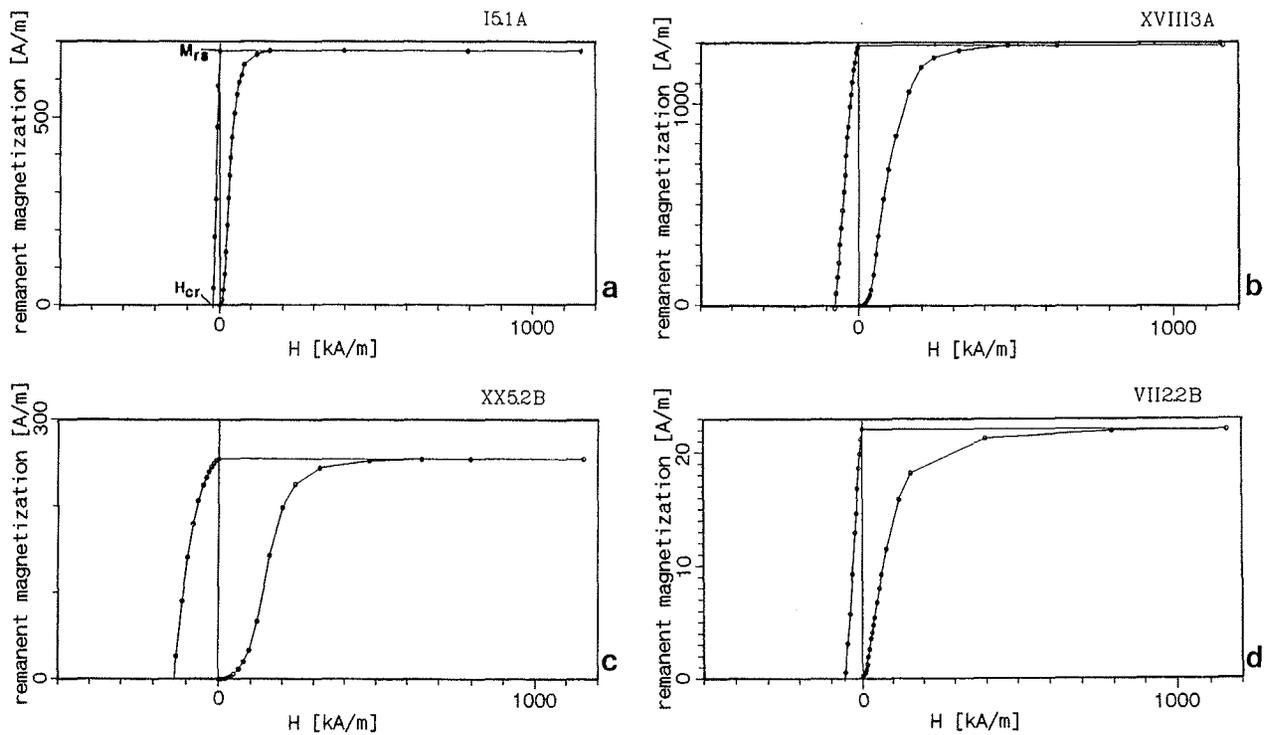
Fig. 8: Representative curves of the isothermal remanent magnetization for the cores from the Shackleton Range dykes. M_{RS} = remanent saturation magnetization; H_{CR} = remanent coercivity.

Abb. 8: Typische Kurvenverläufe isothermaler remanenter Magnetisierungen für die Kernproben der Shackleton-Range-Gänge. M_{RS} = remanente Sattigungsmagnetisierung; H_{CR} = remanente Koerzitivfeldstärke.

Under the microscope it can be seen that the original titanomagnetites in these samples are very strongly or completely altered, the alteration products including Ti-hematite (Tab. 4b). The low content of ferrimagnetic minerals and thus the low saturation remanence of less than 10 A/m (Tab. 3) are due to the fact that they were replaced by paramagnetic minerals.

The M_{RS}/M_S and H_{CR}/H_C ratios allow a diagnosis of the magnetic domain structure. The ratios are plotted against each other in Fig. 10. The boundaries between the fields of SD, PSD and MD particles of titanomagnetite ($Fe_{3-x}Ti_xO_4$ with x = 0.6) are also shown (DUNLOP 1981). Most of the points lie in the PSD field, and some on the boundary between PSD and SD fields.
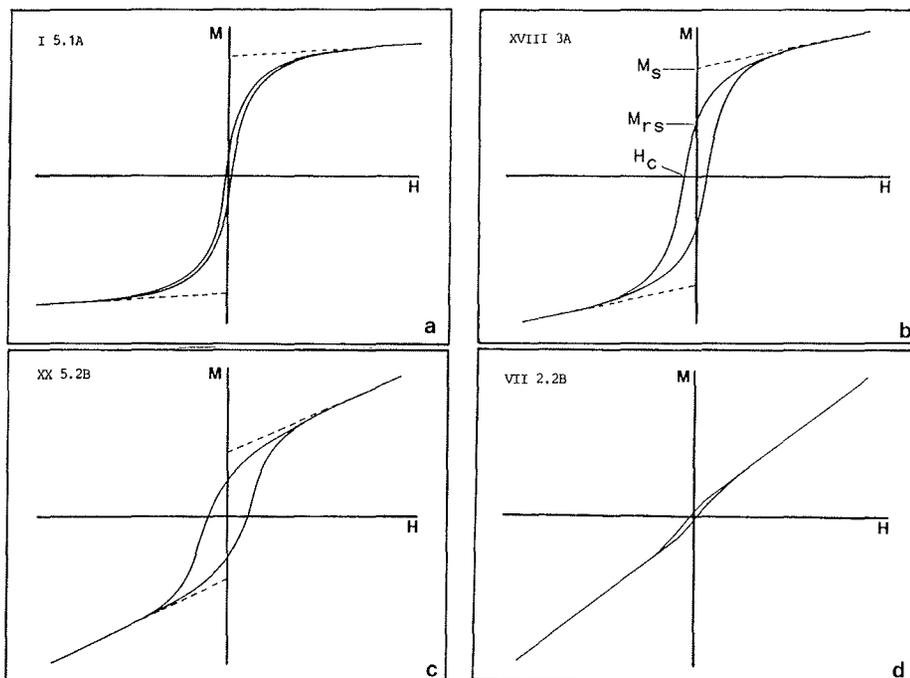

Fig. 9: Representative hysteresis loops for the cores from the Shackleton Range dykes. The maximum field strength (a - d) is 800 kA/m. M_S = saturation magnetization; H_C = coercivity; M_{RS} = remanent saturation magnetization.

Abb. 9: Typische Verläufe von Hysterese-Schleifen fur die Kernproben der Shackleton-Range-Gänge. Die maximale Feldstärke (a - d) beträgt 800 kA/m. M_S = Sättigungsmagnetisierung; M_{RS} = remanente Sättigungsmagnetisierung; H_C = Koerzitivfeldstärke.

Dyke No	Sample No	M_{RS} (A/m)	remanten hyst. H_{CR} (kA/m)	$H_{CR'}$ (kA/m)	H_{CR}/H_{CR}	M_{RS}/M_S	H_{CR}/H_C	Susc. 10^{-6}(SI)	Qmod (A/m)	probable magnetic carrier
Group I										
16a	IV 2A	900.8	50.3	65.1	1.294	0.370	1.397	10106	372.0	TiMa, PSD
16.b	XIX 2B	1058.6	68.3	84.4	1.236	0.432	1.525	8281	419.6	TiMa, PSD
	XIX 4.1B	809.9	59.0	74.1	1.256	0.403	1.639	7300	392.0	TiMa, PSD
25	XX 3B	281.8	146.0	158.5	1.086	0.610	1.443	1353	1357.3	TiMa, Ham SD-P
	XX 5.2B	254.6	136.4	150.7	1.105	0.650	1.451	1263	1171.4	TiMa, Ham SD-P
Group II										
15	XII 3.1A	1196.3	51.2	66.4	1.297	0.265	2.286	1984	90.1	TiMa, PSD
19	XVI 1A	916.1	31.7	41.3	1.302	0.307	1.617	15148	28.2	TiMa, PSD
21	XVI 3.2B	1042.3	36.0	47.3	1.311	0.322	1.552	16286	29.8	TiMa, PSD
	XVI 5B	924.8	37.8	49.7	1.314	0.338	1.524	12798	38.6	TiMa, PSD
23	XVII 1B	854.0	37.5	49.4	1.317	0.349	1.512	11966	46.3	TiMa, PSD
	XVII 3.2B	721.2	36.8	49.2	1.337	0.331	1.484	10155	49.0	TiMa, PSD
	XVII 4B	565.9	40.2	52.6	1.310	0.358	1.621	8596	21.0	TiMa, PSD
24	XVIII 2.2A	1069.2	57.1	75.9	1.330	0.426	1.586	9331	39.5	TiMa, PSD
	XVIII 3A	1286.9	74.8	92.2	1.233	0.495	1.461	9837	14.8	TiMa, PSD
27	XXI 5.1A	424.5	24.8	35.9	1.447	0.173	2.696	20954	22.5	TiMa, PSD
Group IV										
1	I 1A	461.3	19.9	29.6	1.488	0.128	2.487	30837	17.6	TiMa<<Ti, PSD
	I 5.1A	674.9	21.6	31.3	1.449	0.137	2.455	40159	23.1	TiMa, PSD
2	II 3A	163.9	37.1	43.2	1.164	0.218	2.728	1339	42.1	TiMa, PSD
7	VII 2.2B	22.1	57.6	76.2	1.323	-	-	745	34.9	PM
	VII 4.1B	2.3	70.5	55.9	0.793	-	-	652	10.9	PM
8	VIII 1B	1013.2	21.5	31.2	1.451	0.185	1.920	39330	37.8	TiMa, PSD
	VIII 2B	877.0	25.0	35.8	1.433	0.226	1.736	25463	46.5	TiMa, PSD
9	IX 1.1B	125.6	20.2	26.6	1.317	0.192	2.295	5023	33.1	TiMa, PSD
	IX 4.2A	77.3	53.4	53.4	1.000	-	-	1313	40.2	PM
11	X 1.1B	11.9	32.2	42.4	1.317	-	-	1222	14.5	PM
	X 3A	91.9	44.9	59.0	1.314	0.238	3.621	3683	17.7	TiMa, PSD
12	XI 1A	10.3	35.5	41.5	1.169	-	-	968	32.2	PM
13	XII 1.1A	589.6	18.1	26.9	1.496	0.121	2.382	33331	33.0	TiMa<<Ti, PSD
	Xii 4.1A	451.6	55.7	73.1	1.312	0.249	3.027	12940	28.8	TiMa, PSD
Group V										
5	V 2.1A	766.9	30.9	41.9	1.357	0.152	2.664	30337	23.7	TiMa, PSD
	V 3.1A	833.0	19.9	28.6	1.437	0.117	2.487	53661	19.8	TiMa, PSD
6	VI 2A	90.4	26.0	34.5	1.326	0.224	2.321	4091	29.9	TiMa, PSD

Tab. 3: Rock magnetic parameters of the Shackleton Range basalts. M_s = saturation magnetization; M_{RS} = saturation remanence; H_c: coercivity; H_{CR} = remanence coercivity; $H_{CR'}$: H_{CR} at $1/2M_{RS}$; Susc. = initial susceptibility; Q_{mod} = modified Königsberg ratio (see text); TiMa = titanomagnetite (may be maghemitized); TiMa << Ti = TiMa with very low titanium; PM = paramagnetized material, little or no ferrimagnetic material; Häm = hematite; SD = single-domain particles; PSD = pseudo single-domain particles.

Tab. 3: Gesteinsmagnetische Parameter der Shackleton-Range-Basalte. M_s = Sättigungsmagnetisierung, M_{RS} = Sättigungsremanenz, H_c = Koerzitivfeldstärke, H_{CR} = remanente Koerzitivfeldstärke, $H_{CR'}$: H_{CR} bei $1/2$ M_{RS}, Susc = Anfangssuszeptibilität, Q_{mod} = modifiziertes Königsberger-Verhältnis (vgl. Text), TiMa = Titanmagnetit (kann maghemitisiert sein), TiMa<<Ti = TiMa mit sehr geringem Titananteil, PM = paramagnetischer, kaum ferrimagnetischer Anteil, Häm = Hämatit, SD = Singledomain-Teilchen, PSD = Pseudo-Singledomain-Teilchen.

MD structures are never dominant and because of their low abundance are not represented in Fig. 10. It is postulated that, due to the magnetic stability of PSD particles, the magnetization, i.e. the TRM and possibly a CRM, have remained almost completely unchanged since they were generated.

Summarizing, it can be said that groups I and II (northern and northwestern parts of the Shackleton Range), since they contain secondary minerals due to hydrothermal alteration (the age of which is not known) probably possess a CRM that is possibly superimposed upon the TRM. Only after the demagnetization
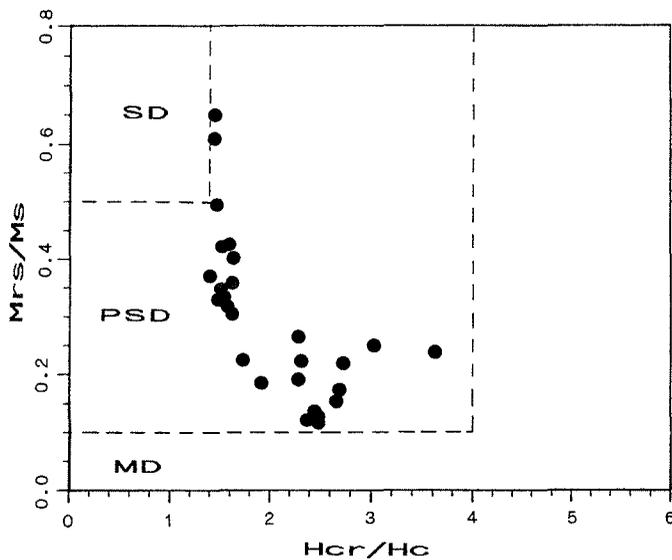
Fig. 10: M_{RS}/M_S versus H_{CR}/H_C showing areas of single domain (SD), pseudo single domain (PSD), and multidomain titanomagnetite grains after DUNLOP (1981).

Abb. 10: Darstellung der Verhältnisse M_{RS}/M_S gegen H_{CR}/H_C mit Bereichen für Einbereich- (SD), Pseudoeinbereich- (PSD) und Mehrbereich-Titanmagnetitkörnern nach DUNLOP (1981).

values are available will it be possible to find out whether the CRM was acquired autohydrothermally after the TRM, or whether it is due to more recent hydrothermal activity and is possibly associated with a modified magnetic direction. At least dyke 16a (group I) probably displays a primary direction, since no secondary ferrimagnetic or antiferromagnetic minerals were identified.

The presence of secondary ferrimagnetic or antiferromagnetic minerals suggests that the dykes of groups IV and V (Read Mountains) contain components which are possibly partly or completely superimposed upon the primary TRM. At least in the cores from dykes 5 and 8, the primary titanomagnetites seem to be completely altered. The presence of these secondary minerals means that the ChRM direction of these dykes probably no longer corresponds to the primary ChRM acquired during the cooling phase of the rock melt, but to a ChRM acquired at a later but unknown date.

3. DETERMINATION OF THE CHARACTERISTIC REMANENT MAGNETIZATION DIRECTIONS

The characteristic remanent magnetization (ChRM) directions determined on the basis of demagnetization are often influenced by a number of factors which may lead to deviation of the measured remanent magnetization direction from the true palaeo-direction.

Among these factors is the impact of tectonic stress on the dykes; its influence is discussed in detail by HOTTEN (1993). The general orientation and relationships between dykes and coun-

try rock suggest that none of the dykes from which samples were taken for palaeomagnetic studies had been subjected to external rotation or tilting. Slight tilting cannot definitely be excluded. It is, however, not quantifiable. The same is true for internal deformation, indications of which were found in only one of the dykes from which samples were taken for palaeomagnetic studies (epidote-covered slickensides in dyke 9). Therefore, no tectonic correction was applied to any of the dykes.

Other natural or experimental sources of error cause a scattering of the values, the extent of which is indicated by the precision parameter k and the α_{95} confidence interval (FISHER 1953).

To calculate these values - even before using Fisherian statistics - the average ChRM is taken of two demagnetized sections of the same rock core and then that of all cores from the same specimen. For this reason, only one direction per specimen was used for Fisherian statistics, irrespective of the number of individual cores per specimen. Although 268 cores were investigated, i.e. 12 to 13 cores per dyke on average, the sometimes high α_{95} values reflect the comparably few (3 to 7) rock samples taken from each dyke.

To carry out a true statistical analysis of the demagnetization results, more closely spaced sampling of the mafic dykes would have been desirable, but was not possible because of lack of time and because transport capacity during the expedition was limited.

For these reasons and irrespective of the confidence interval, those ChRMs with a precision parameter k >10 are included in data evaluation and interpretation (>10 suggests that the average is very close to the true value (FISHER 1953).

3.1 The ChRM of mafic dykes of basalt group I (northern Shackleton Range)

This group comprises dykes 16a, 16b and 25. The cores from dykes 16a and 16b show a very similar demagnetization behaviour, whereas those from dyke 25 show significant differences. The demagnetization results are given in Table 4.

The results of NRM measurements before and after storage for four weeks (shielded against external magnetic fields) indicate that the cores possess a very low magnetic viscosity. In some cases, a loss in intensity of up to 2 % can be observed; NRM declination and inclination show differences of up to 40 and 20, respectively. This is a further indication that multi-domain particles are by no means abundant.

Dykes 16a and 16b show high NRM intensities and average susceptibilities. High MDF values (Mean Destructive Field) provide evidence of the high alternating-field stability of the cores (Tab. 4; Tabs. 4 and 5 both show NRM intensities after storage).

Figs. 11 and 12 show the results from two sections of the same

Dyke		Susceptibility x 10^{-6} (SI)		NRM (mA/m)		MDF (kA/m)		decl. (°)	incl. (°)	Plat (°)	Plong (°)	P	N$_H$	k	α_{95} (°)

Group I

16a	12293	(8631-17192)	2518	(1777-3759)	45.1	(19.1-78.2)	41.0	-60.7	48.7S	200.1S	+	6	320.4	3.7
16b	7566	(6825- 8281)	2947	(2573-3577)	76.9	(63.6-88.1)	48.1	-62.3	49.6S	208.4E	+	3	101.1	12.3
25	1317	(1263- 1396)	1682	(1464-1915)	162.2	(154.2-166.5)	4.4	-23.3	21.8S	21.8E	+	4	6.1	40.7

Group II

15	22042	(18360-27615)	1605	(714-2042)	27.9	(13.4-65.3)	65.6	46.4	23.4S	32.9E	-	5	102.6	7.6
19	15014	(12119-16598)	493	(346- 609)	17.5	(15.4-19.8)	28.0	61.7	34.3S	335.3E	-	3	125.1	11.1
21	14897	(12732-16588)	501	(455- 586)	16.0	(10.9-20.0)	6.5	59.5	30.8S	336.4E	-	5	14.3	20.9
23	10141	(8915-12135)	401	(180- 600)	13.6	(10.3-15.8)	35.1	62.0	35.2S	9.6E	-	4	44.7	7.3
24	9403	(906-10787)	283	(146- 375)	49.0	(24.9-95.1)	19.4	42.3	15.4S	349.0E	-	4	44.5	13.9
27	16531	(906-22784)	431	(69- 643)	24.6	(02.1-75.9)	39.6	63.5	37.2S	8.8E	-	6	87.3	7.2

Tab. 4: Palaeomagnetic data for the dykes in the northern and northwestern Shackleton Range. NRM = natural remanent magnetization; MDF = mean destructive field. The mean values are given for each of these parameters, with the range in parentheses. decl/incl = declination/inclination of the characteristic remanent magnetization; P_{lat}/P_{long} = latitude/longitude of the virtual geomagnetic pole; p = polarity; +/- = normal/inverse polarity; N_H = number of statistically interpreted hand samples; k and α_{95} = statistical parameters after FISHER (1953).

Tab. 4: Paläomagnetische Ergebnisse der Dykes in den nördlichen und nordwestlichen Gebieten der Shackleton Range. Vor den Klammern sind die arithmetischen Mittelwerte angegeben, innerhalb der Klammern der Wertebereich. NRM = natürliche Remanente Magnetisierung, MDF = Mean Destructive Field, Decl/Incl = Deklination/Inklination der charakteristischen Remanenten Magnetisierungsrichtung, P_{Lat}/P_{Long} = geographische Breite zu Länge des Virtuellen Geomagnetischen Pols, p = Polarität, +/- = normale bzw. inverse Polarität, N_H = Anzahl der statistisch ausgewerteten Handstücke, k und α_{95} = statistische Parameter nach FISHER (1953).

core for comparison; one section was thermally demagnetized, and the other was demagnetized in an alternating field (AF).

The blocking temperature spectrum can be read from the thermal demagnetization curve. In the temperature interval between 250 and 300 °C, a distinct decrease in the magnetization can be recognized. The magnetization also decreases considerably between 540 and 580 °C. This blocking temperature spectrum agrees well with the Curie points determined on the same core: T_{C1} = 279 °C, T_{C2} = 567 °C (see also Tab. 2). It is postulated that T_{C2} is due to exsolution of the primary titanomagnetites (T_{C1}) associated with deuteric high-temperature oxidation and took place during cooling of the intruded rock.

In the Zijderveld diagram (Fig. 11, bottom left) and in the stereographic projection (right), both titanomagnetite fractions show identical remanence directions. An unstable component which deviates only slightly from the stable direction is removed at a temperature of 200 °C. As the magnetization decreases further, the magnetization vector describes a nearly straight line to the origin of the Zijderveld diagram. The direction of magnetization remains stable within both blocking temperature intervals. These results suggest that both residually magnetized mineral phases are of the same geological age and have a primary TRM. The small amount of hydrothermal titanohematite that can be seen in the polished section are not reflected in the demagnetization curve.

The declination and inclination vectors of the stable direction, which are very close together, can be seen in the right-hand diagram in Fig. 11.

The results of the AF demagnetization (Fig. 12) show very good agreement with the results of thermal demagnetization. The direction and difference vectors become stable at the third step of demagnetization.

The other cores from dykes 16a and 16b yielded similar results. The average ChRM declination and inclination values and the geographical latitude (Lat) and longitude (Long) of the virtual geomagnetic poles (VGPs) calculated from Lat and Long are shown in Table 4. The scatter of the data for each of the two dykes is insignificant so that high values are obtained for k.

Completely different behaviour is shown by dyke 25. The susceptibility (approximately 1300 x 10^{-6}) is considerably lower (Table 4); the NRM (about 1700 mA/m on average) attains only slightly lower values than for the other dykes of this basalt group. MDF values are about twice to three times as high, however, and indicate that the stability of the magnetization is much greater. The ChRM directions for this dyke, which were also obtained by thermal and alternating-field demagnetization, show considerable scatter (k = 6.1). It was not possible to explain this behaviour on the basis of rock magnetism (HOTTEN 1993). On account of the low k value (k <10), the ChRM of this dyke is left out of further consideration.

ChRM directions and VGP positions of dykes 16a and 16b are shown in Fig. 13. The stable directions of both dykes show normal polarity. The averaged pole is 49.2 °S, 204.2 °E. As this value was averaged from only two VGPs, further statistical analysis is not possible.
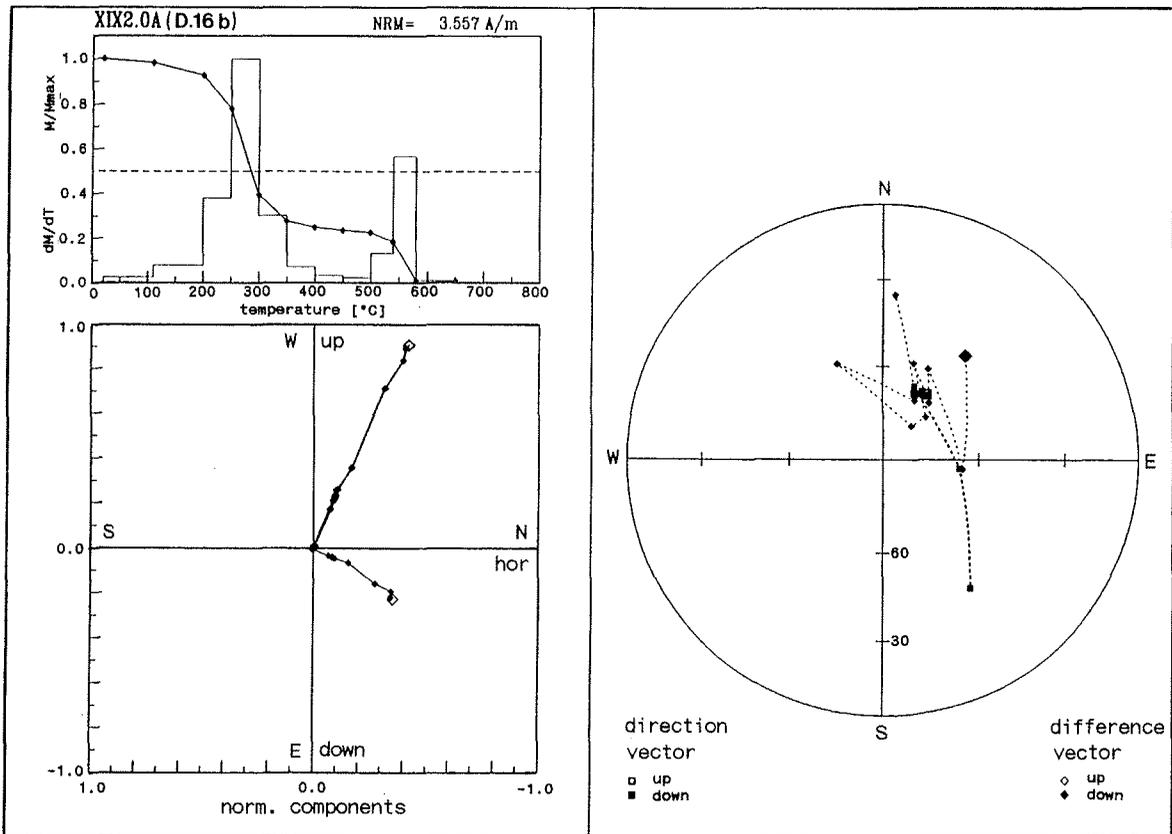
Fig. 11: Demagnetization behavior of cores from dyke 16b. Top left = demagnetization curve (bold line, normalized with respect to the maximum magnetization) and the ratio of the change of magnetization to progressive change in temperature in each measuring interval (thin line); bottom left = Zijderveld diagram showing inclination (bold line) and declination (thin line); right = stereographic projection of the magnetic direction vectors (squares, bold lines) and difference vectors (rhombs, thin lines). The initial directions are marked by larger symbols. Dashed line = lower hemisphere; solid line: upper hemisphere

Abb. 11: Entmagnetisierungsverhalten von Kernproben aus Dyke 16b. Links oben = Entmagnetisierungskurve (dicke Linie, normiert auf den Maximalwert) und Quotient aus Magnetisierungsänderung und progressiver Temperaturänderung in jedem Meßintervall (dünne Linie); links unten = Zijdervelddiagramm mit Darstellung der Inklination (dicke Linie) und Deklination (dünne Linie); rechts = Lagekugelprojektion der Richtungsvektoren (Quadrate, dicke Linien) und Differenzvektoren (Rauten, dünne Linien). Die Anfangsrichtungen sind durch größere Symbole gekennzeichnet. Gestrichelte Linie = untere Halbkugel; durchgezogene Linie = obere Halbkugel.

3.2 The ChRM of mafic dykes of group II (northern part of Shackleton Range)

The demagnetization results are given in Table 4. In spite of the considerably stronger hydrothermal alteration of the rocks of this group, it was possible to determine the VGPs of all six dykes with sufficient precision (k: 14-125, Tab. 4). Magnetic studies have already shown distinct differences from the dykes of group I. These differences are also reflected in the demagnetization behaviour of the cores.

As with the basalts of group I, storage caused only minor changes in the NRM. Only in one case (dyke 27) were major differences found (intensity of magnetization fell by a maximum of 9 % compared to the time before storage; differences between declination and inclination values before and after storage were 80 and 50 at a maximum, respectively).

In comparison, the average susceptibilities are high: about 9.4 x 10^{-3} and 22 x 10^{-3} (Tab. 4). The NRM values in this rock group are considerably lower; except for dyke 15, they are much

below 1000 mA/m. These magnetization intensities, which are low for basalts, are probably due to the advanced degree of alteration of the titanomagnetites. That the magnetization is also often less stable, can be seen from the MDF values, which are generally lower than those of basalt group I.

The six dykes of this group can be subdivided according to their demagnetization behaviour into
a) dykes whose cores attain stable directions in the course of demagnetization, from which a mean site ChRM can be obtained; and
b) dykes whose cores only partly attain a stable direction or do not attain one at all, but for which with increasing demagnetization the points move along converging great circles on the projection (remagnetization circles, KHRAMOV 1958).

The results of demagnetization of the dykes listed under a), i.e. dykes 15, 19, and 27, were evaluated in the same way as those of group I dykes. To determine a stable direction of magnetization for the dykes listed under b), i.e. dykes 21, 23, and 24, another method was applied, which will be explained later.
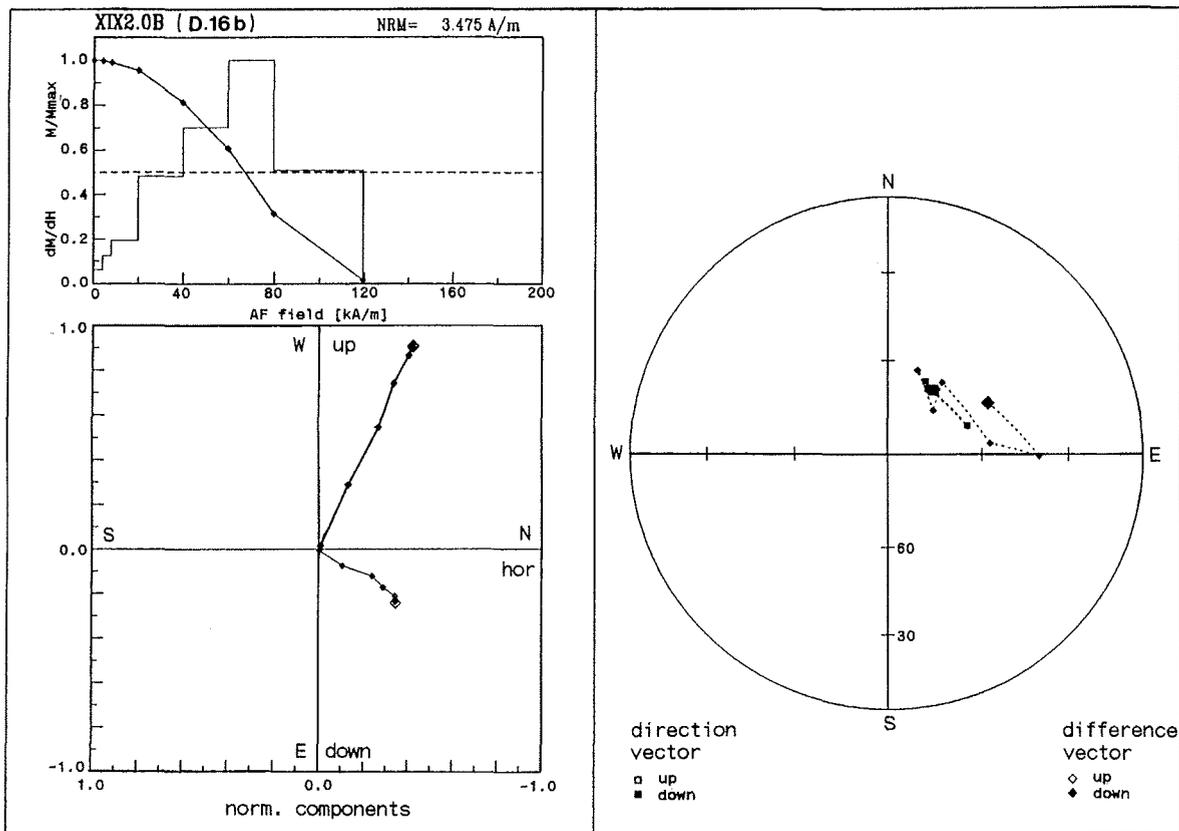
Fig. 12: Demagnetization behavior of cores from dyke 16b. Top left = demagnetization curve (bold line, normalized with respect to the maximum magnetization) and the ratio of the change in magnetization to alternating field in each measuring interval (thin line); bottom left = Zijderveld diagram showing inclination (bold line) and declination (thin line); right = stereographic projection of the magnetic direction vectors (squares, bold lines) and difference vectors (rhombs, thin lines). The initial directions are marked by larger symbols. Dashed line = lower hemisphere; solid line= upper hemisphere.

Abb. 12: Entmagnetisierungsverhalten von Kernproben aus Dyke 16b. Links oben = Entmagnetisierungskurve (dicke Linie, normiert auf den Maximalwert) und Quotient aus Magnetisierungsänderung und Wechselfeldänderung in jedem Meßintervall (dünne Linie); links unten = Zijdervelddiagramm mit Darstellung der Inklination (dicke Linie) und Deklination (dünne Linie); rechts = Lagekugelprojektion der Richtungsvektoren (Quadrate, dicke Linien) und Differenzvektoren (Rauten, dünne Linien). Die Anfangsrichtungen sind durch größere Symbole gekennzeichnet. Gestrichelte Linie = untere Halbkugel; durchgezogene Linie = obere Halbkugel.

Figs. 14 and 15 show the results of one thermally demagnetized core and one core demagnetized in an alternating field, both of which attained stable directions.

The blocking temperature spectrum in Fig. 14 shows two maxima, one between 300 and 330 °C and the other between 540 and 600 °C. In addition to primary, maghemitized and partly hydrothermally altered titanomagnetite, fine-grained, probably secondary (titano-?)magnetite was determined as remanence carrier; no hydrothermal alteration or oxidation were recognizable in the latter, possibly due to the very small grain size. Hydrothermal alteration to titanohematite was also found. The two blocking temperature maxima are caused by magnetite and/or titanomagnetite of variable composition and degree of oxidation, and titanohematite.

In the Zijderveld diagram and stereographic projection of this core (Fig. 14), it can be seen that an unstable magnetization component disappears at about 200 °C, i.e. far below the first blocking temperature maximum. The direction vector then remains almost stationary up to 540 °C. At 570 °C, there is a

residual magnetization of over 20 %, which is due to the presence of titanohematite. During the last two demagnetization steps (570 and 600 °C), the direction vector changes its position. In this case the remanent magnetization direction of the minerals with blocking temperatures between 540 and 600 °C, probably secondary minerals, is different from that of the magnetization carrier with blocking temperatures between 300 and 330 °C.

Fig. 15 documents the alternating field demagnetization of a specimen: Initially, a distinct, low stability remanent magnetization gradually disappears leaving only the magnetically more stable component. This behaviour is clearer in the Zijderveld diagram. The direction of magnetization whose vector components do not move towards the origin with increasing alternating field strength, begins to change at about 8 kA/m (fourth demagnetization step).

At about 16 kA/m (eighth demagnetization step) the more unstable magnetization component is removed. With further decreasing remanence, the magnetization directions move directly towards the origin.
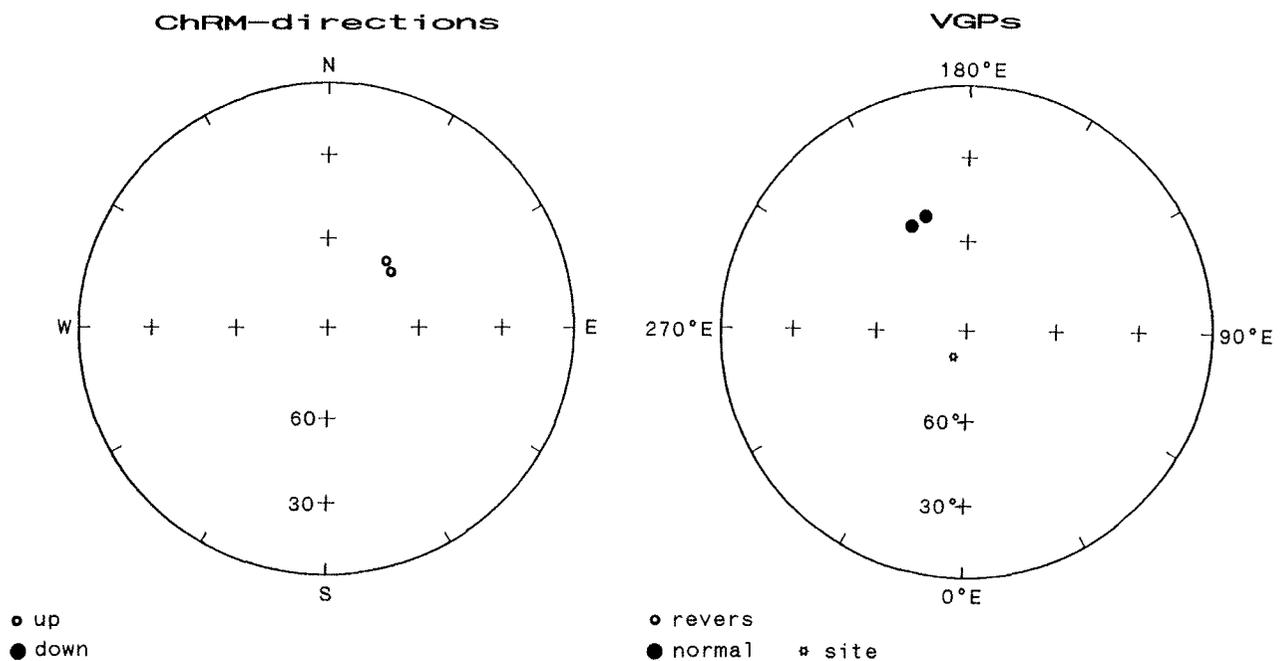
137

ChRM-directions

N

o up
● down

VGPs

o revers
● normal   ¤ site

Fig. 13: ChRM directions and VGPs for dykes of Group I. ChRM directions are plotted on a Schmidt net; VGPs are plotted in a polar stereographic projection (lower hemisphere; projection plane = equator).

Abb. 13: ChRM-Richtungen und VGPs für Gänge der Gruppe I. Darstellung der ChRM-Richtungen im Schmidtschen Netz; Darstellung der VGPs in einer polständigen, flächentreuen stereographischen Projektion (untere Halbkugel; Projektionsebene = Äquatorebene).

The two remanent magnetization vectors point in opposite directions so that the intensity of magnetization of the core increases with destruction of the less stable component. This increase in intensity becomes evident in the demagnetization curve (top left in the figure) between the third and the eighth demagnetization steps. Only after the less stable component has been completely removed, does AF demagnetization cause a loss of intensity again.

The stereographic projection shows the „migration" of the direction vector during the first eight demagnetization steps (Fig. 15, right). After the eighth demagnetization step, the difference vector, too, approaches a stable direction at a declination and inclination of about 45° and 68°, respectively, in this example.

The ChRM directions of the dykes mentioned above under b) had to be determined using another method, since stable directions were seldom achieved during demagnetization:

It can be seen in the projection in Fig. 15 that the magnetization directions move along a great circle during the stepwise destruction of the less stable magnetization component. In the example shown here, a stable final point was reached. In some cases, no stable direction is ever reached. This results from the superimposition of the coercive field strength or blocking temperature spectra of various remanent magnetizations. This is true when the spectra overlie each other over their entire width and both components are destroyed concurrently; this is also true

when the spectra do not completely overlie each other, but the magnetization intensity is so low after demagnetization of the less stable remanent magnetization that the direction of the more stable magnetization component cannot any longer be determined with the magnetometer used for these studies. If the great circles containing the directions measured after each demagnetization step for several cores from one dyke converge towards the same direction, a ChRM can be defined from the points of intersection of these „remagnetization circles" (HALLS 1976, 1978).

The demagnetization data for dykes 21, 23, and 24 were evaluated as described by HOTTEN (1993) in detail.

Fig. 16 shows the ChRM directions and VGPs of these six dykes. In all cases, an inverse direction of magnetization was obtained. The precision parameter k ranges between about 14 and 125, and the confidence angle between about 7° and 21° (Tab. 4). The mean position of the paleopole determined on the basis of the VGPs of the dykes of this basalt group is 30.8 °S, 1.9 °E (k = 18.2, α_{95} = 16.1°)

3.3 The ChRMs of mafic dykes of groups IV and V (Read Mountains)

The results of demagnetization of cores drilled from eight mafic dykes belonging to group IV and two mafic dykes from group V are listed in Table 5.
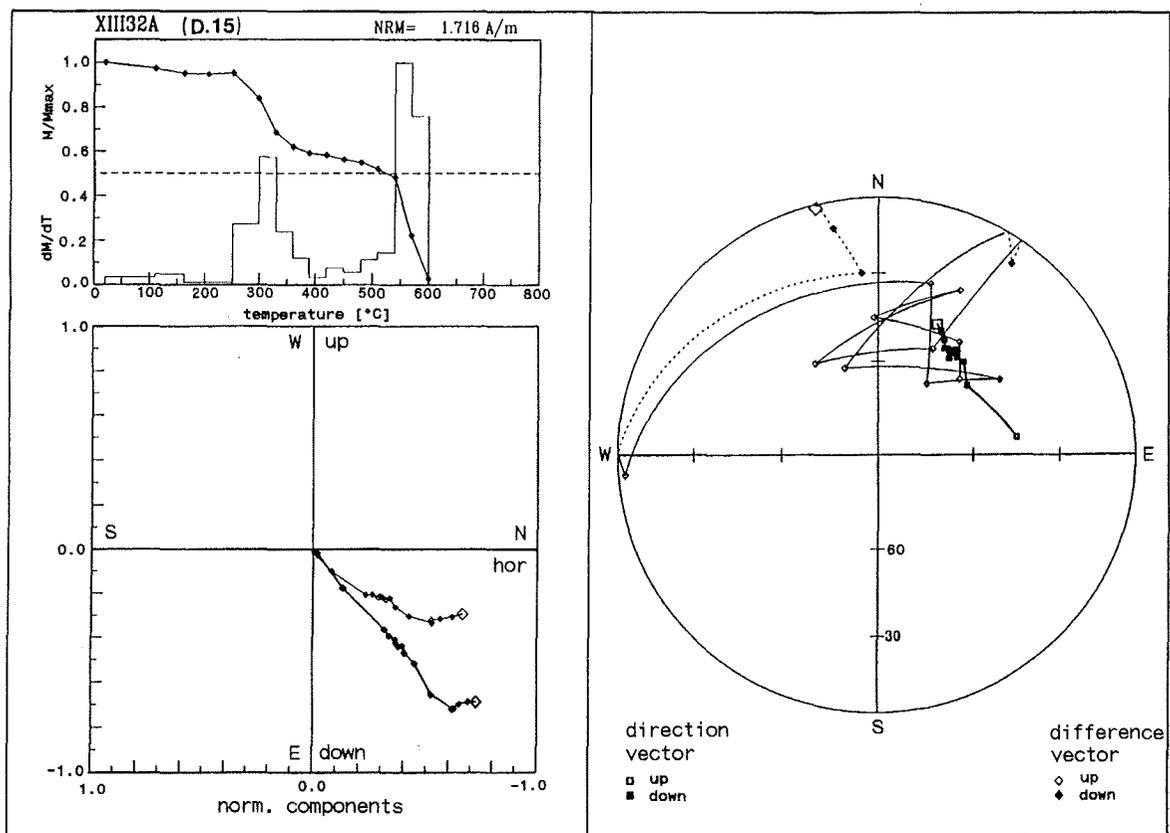
Fig. 14: Demagnetization behavior of cores from dyke 15. Top left = demagnetization curve (bold line, normalized with respect to the maximum magnetization) and the ratio of the change in magnetization to progressive change in temperature in each measuring interval (thin line); bottom left = Zijderveld diagram showing inclination (bold line) and declination (thin line); right = stereographic projection of the magnetic direction vectors (squares, bold lines) and difference vectors (rhombs, thin lines). The initial directions are marked by larger symbols. Dashed line = lower hemisphere; solid line = upper hemisphere.

Abb. 14: Entmagnetisierungsverhalten von Kernproben des Dyke 15. Links oben = Entmagnetisierungskurve (dicke Linie, normiert auf den Maximalwert) und Quotient aus Magnetisierungsänderung und progressiver Temperaturänderung in jedem Meßintervall (dünne Linie); links unten = Zijdervelddiagramm mit Darstellung der Inklination (dicke Linie) und Deklination (dünne Linie); rechts = Lagekugelprojektion der Richtungsvektoren (Quadrate, dicke Linien) und Differenzvektoren (Rauten, dünne Linien). Die Anfangsrichtungen sind durch größere Symbole gekennzeichnet. Gestrichelte Linie = untere Halbkugel; durchgezogene Linie = obere Halbkugel.

The magnetic viscosity of most of the cores of the Read Mountain basalt dykes is low. However, some samples show relatively large NRM differences before and after storage. For example, the maximum loss of intensity for Dyke 12 is 16 %; the maximum declination and inclination differences are 54° and 24° respectively. This behavior suggests that a relatively high proportion of multidomain particles are present.

The susceptibility, NRM, and MDF of the basalts cover a wide range. The NRM intensities vary between 17 and 1500 mA/m (means of all core samples from a single dyke, Tab. 5) whereas susceptibilities range from about 760 x 10⁻⁶ to more than 38,000 x 10⁻⁶. Most of the MDF values are about 10 kA/m or less and indicate less stable remanent magnetization. The wide range of values cannot be explained exclusively by differences in the primary mineral composition of the dykes. It is probably based on the following two factors: (a) Progressive low temperature oxidation or hydrothermal alteration of the primary ferrimagnetic minerals; the mineral susceptibilities and intensities of magnetization are reduced to different degrees depending on the degree of alteration. (b) Secondary, newly formed ferrimagne-

tic or antiferromagnetic ore minerals have CRMs which are superimposed on the primary, initial TRM and result in increased magnetic intensity.

Ore microscopy and rock magnetic measurements show that the two processes occurred in all dykes in the Read Mountains, but to different extents. The following examples explain this.

Dykes 7 and 12 show extremely low values of susceptibility and NRM (Tab. 5). In both cases, primary, exsolved titanomagnetite completely replaced by non-opaque minerals was observed, as well as small amounts of titanohematite (Tab. 1, Fig. 5b). Unaltered magnetite only occurs sporadically as narrow growth rims or more rarely as newly formed crystals. The shape of the thermomagnetic curves reflects the strong hydrothermal alteration of the samples (curve types II.3 and II.5, see Fig. 7). Extremely low saturation remanences (IRM measurement) and hysteresis measurements show that only small amounts of ferrimagnetic or antiferromagnetic minerals have been preserved (Figs. 8d and 9d, Tab. 3) and the influence of secondary ore minerals is low.
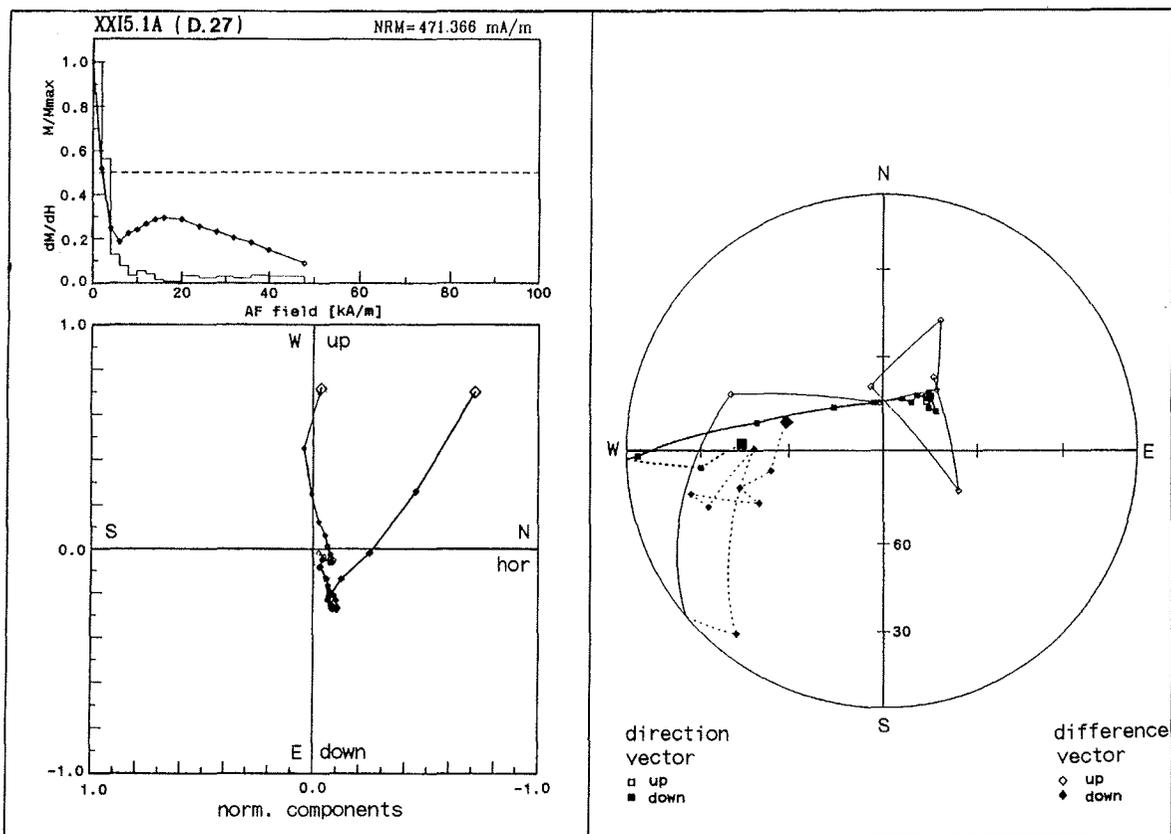
139

Fig. 15: Demagnetization behavior of cores from dyke 15. Top left: demagnetization curve (bold line, normalized with respect to the maximum magnetization) and the ratio of the change in magnetization to alternating field in each measuring interval (thin line); bottom left = Zijderveld diagram showing inclination (bold line) and declination (thin line); right = stereographic projection of the magnetic direction vectors (squares, bold lines) and difference vectors (rhombs, thin lines). The initial directions are marked by larger symbols. Dashed line = lower hemisphere; solid line = upper hemisphere.

Abb. 15: Entmagnetisierungsverhalten von Kernproben des Dyke 15. Links oben = Entmagnetisierungskurve (dicke Linie, normiert auf den Maximalwert) und Quotient aus Magnetisierungsänderung und Wechselfeldänderung in jedem Meßintervall (dünne Linie); links unten = Zijdervelddiagramm mit Darstellung der Inklination (dicke Linie) und Deklination (dünne Linie); rechts = Lagekugelprojektion der Richtungsvektoren (Quadrate, dicke Linien) und Differenzvektoren (Rauten, dünne Linien). Die Anfangsrichtungen sind durch größere Symbole gekennzeichnet. Gestrichelte Linie = untere Halbkugel; durchgezogene Linie = obere Halbkugel.

In contrast, the susceptibilities and NRM intensities of dyke 5 for example are very high. In addition to primary titanomagnetite which is hydrothermally partially altered or completely replaced by titanohematite and non-opaque minerals, a large proportion of fine-grained, secondary magnetite and hematite is present, which were formed with chlorite and serpentine by the almost complete low-grade metamorphic alteration of augite (Fig. 3b). Since the secondary, newly formed magnetite is the dominant carrier of magnetization and not the altered, primary titanomagnetite, the rock magnetic measurements on this dyke (No. 5) show different results to those mentioned above (dykes 7 and 12). The shape of the thermomagnetic curve is considerably influenced by the newly formed magnetite (curve type I.1, Fig. 6). IRM and hysteresis measurements display corresponding differences (Figs. 8a and 9a, Tab. 3).

If, as is inferred, the mafic dykes in the Read Mountains were intruded during the Proterozoic and were later heated, probably during the Ross Orogeny, then different ChRM directions and VGP positions would result. The pole positions are discussed in the next chapter in the light of this.

The dykes can be subdivided into three groups on the basis of their demagnetization behavior; these are independent of the basalt groups IV and V:

Group A: Dykes for which a ChRM direction could not be determined using either thermal or alternating field demagnetization

Group B: Dykes for which it was possible to determine ChRM directions

Group C: Dykes which in some cores show another stable direction in addition to the dominant ChRM direction (Tab. 5)

Dykes 7, 12, and 13 belong to Group A. The demagnetization behavior of dykes 7 and 12 can be attributed to partial recrystallization of the remanent magnetization carrier and the corresponding loss of magnetization (see above). Even if primary magnetization were preserved, it cannot be determined because of the low initial intensity and the rapid loss of intensity during demagnetization (low MDF values).
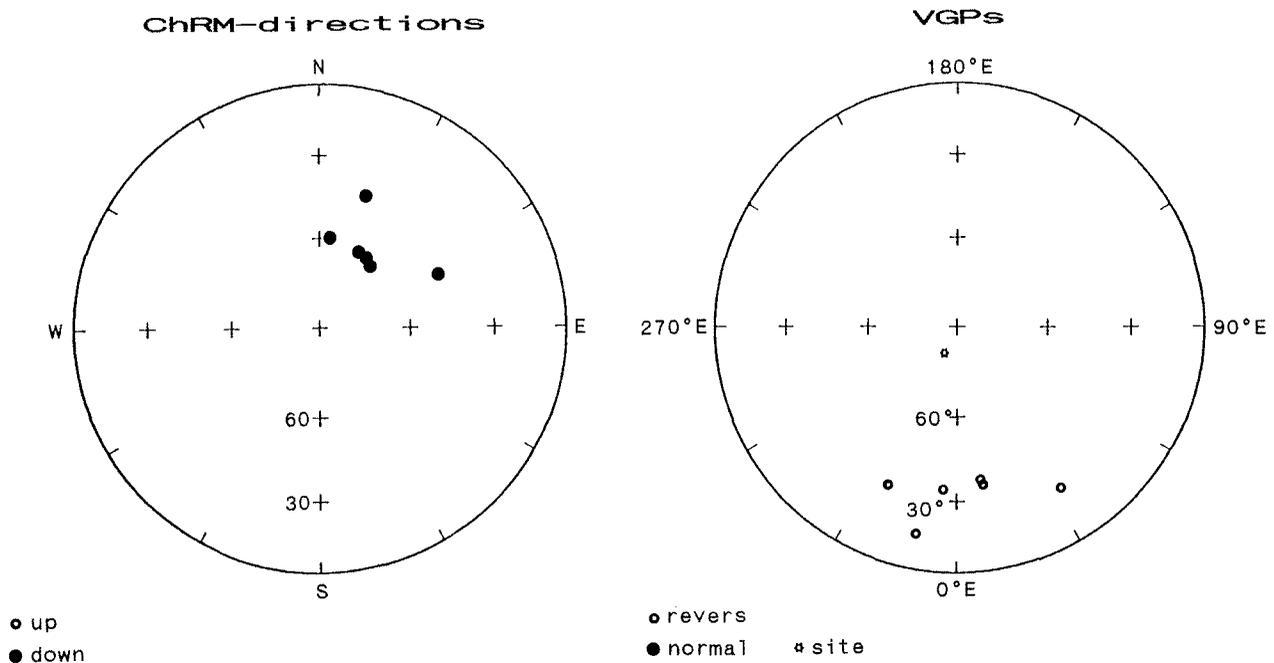
140

Fig. 16: ChRM directions and VGPs for dykes of Group II. ChRM directions are plotted on a Schmidt net; VGPs are plotted in a polar stereographic projection (lower hemisphere; projection plane: equator).

Abb. 16: ChRM-Richtungen und VGPs für Gänge der Gruppe II. Darstellung der ChRM-Richtungen im Schmidtschen Netz; Darstellung der VGPs in einer polständigen, flächentreuen stereographischen Projektion (untere Halbkugel; Projektionsebene = Äquatorebene).

Dyke	Susceptibility x 10⁻⁶ (SI)		NRM (mA/m)		MDF (kA/m)		decl. (°)	incl. (°)	Plat (°)	Plong (°)	P	N$_H$	k	α$_{95}$ (°)
Group IV														
1a	30171	(21743-43768)	640	(437-918)	6.5	(4.7-10.9)	354.2	-3.4	10.9S	148.3E	+	3	8.5	45.2
1b							109.0	-10.0	2.0S	263.7E	+	2	-	-
2	12300	(897-47450)	438	(31-1375)	10.0	(8.3-11.7)	212.6	13.9	14.8S	187.)E	-	3	13.0	35.7
7	795	(652- 886)	17	(7- 35)	36.7	(13.9-59.1)	-	-	-	-	-	-	-	-
8	34836	(25463-39330)	1495	(1184-1819)	8.9	(7.2-11.1)	171.1	-8.6	4.8S	147.6E	-	4	22.6	19.7
9	1313	(923- 5023)	44	(9- 166)	11.3	(4.3-22.8)	247.2	6.7	6.9S	224.4E	-	3	18.6	29.4
11a	3673	(1026-12656)	57	(5- 198)	12.5	(19.7-16.4)	39.9	42.7	17.5S	14.1E	-	4	16.8	23.1
11b							125.0	13.0	11.9S	100.2E	-	2	-	-
12	913	(873-968)	18	(4- 43)	8.5	(6.0-11.9)	-	-	-	-	-	-	-	-
13	25002	(8936-35946)	661	(135-110)	7.5	(6.7- 9.9)	-	-	-	-	-	-	-	-
Group V														
5a	38321	(21789-64743)	878	(422-1724)	8.1	(6.3-10.5)	220.9	-36.7	13.3S	14.3E	+	5	29.0	14.4
5b							294.0	-1.0	4.3S	88.8E	+	2	-	-
6	39897	(3062-5182)	159	(75-3350)	7.1	(5.1- 8.5)	223.8	-28.6	8.5S	17.6E	+	2	-	-
Granodiorite														
29	254			(196-335)	0.32	(014- 051)								

Tab. 5: Palaeomagnetic results of the Read Mountains Dykes. NRM = natural remanent magnetization; MDF = mean destructive field. The mean values are given for each of these parameters, with the range in parentheses. decl/incl = declination/inclination of the characteristic remanent magnetization; P$_{lat}$/P$_{long}$ = latitude/longitude of the virtual geomagnetic pole; p = polarity; +/- = normal/inverse polarity; N$_H$ = number of statistically interpreted hand samples; k and α$_{95}$ = statistical parameters after FISHER (1953). (a) and (b) = Two different directions determined on the core samples of a dyke.

Tab. 5: Palaomagnetische Ergebnisse der Read Mountains Dykes. Vor den Klammern sind die arithmetischen Mittelwerte angegeben, innerhalb der Klammern der Wertebereich. NRM = natürliche Remanente Magnetisierung, MDF = Mean Destructive Field, Decl/Incl = Deklination zu Inklination der charakteristischen Remanenten Magnetisierungsrichtung, P$_{Lat}$/P$_{Long}$ = geographische Breite zu Länge des Virtuellen Geomagnetischen Pols, p = Polarität; +/- = normale bzw. inverse Polarität, N$_H$ = Anzahl der statistisch ausgewerteten Handstücke, k und α$_{95}$ = statistische Parameter nach FISHER (1953). a) und b) bezeichnen zwei unterschiedliche, an den Kernproben eines Ganges ermittelte Richtungen.

No mean ChRM direction could be determined for dyke 13, although these samples show relatively high NRM intensities. Most of the individual cores showed stable directions; however, some cores, even from one single sample, show different directions, with positive and negative inclinations, covering most possible directions in space. Some directions correspond to the present direction of the earth's magnetic field. The stability of the remanent magnetization is low (MDF = 7.5 kA/m). Microscopic examination showed coarse-grained titanomagnetite up to 1.4 mm across. The unfavorable demagnetization behavior of this dyke possibly due to a relatively large content of multidomain particles.

The ChRM directions of the dykes of Groups and B and C are the result of the determination of stable end points and analyses of great circles. Generally, the demagnetization behavior and results are less clear than those of the dykes of the northern and northwestern parts of the Shackleton Range, which have not been affected by metamorphism and whose ore minerals are less altered. In some cases, neither alternating-field nor thermal demagnetization of cores produced stable directions or circles

of remagnetization. It was not possible to explain this behavior. These samples were not taken into consideration when determining the mean ChRM of the relevant dyke. Some of the directions in Table 5 are defined using less than three rock samples; thus it was not possible to use Fisherian statistics. These directions cannot be considered to be ChRMs in the strict sense. They are of interest for interpretation of the results (see below), but they should only be used as auxiliary data.

The results of thermal demagnetization are shown in Figs. 17 and 18. The two cores have a more or less continuous blocking temperature spectrum. In the case of core V3.2B (Fig. 17), a stable direction occurs at 100 °C (see direction and difference vectors); the magnetization remaining above 570 °C (about 22 %) is due to hematite.

The behavior of the direction vector of core X3.0B is different (Fig. 18). At the beginning of demagnetization, the inclination values are very low. However, the direction vector changes until the declination becomes stable at about 52°and the inclination at about 570 after the fifth magnetization step (400 °C). This
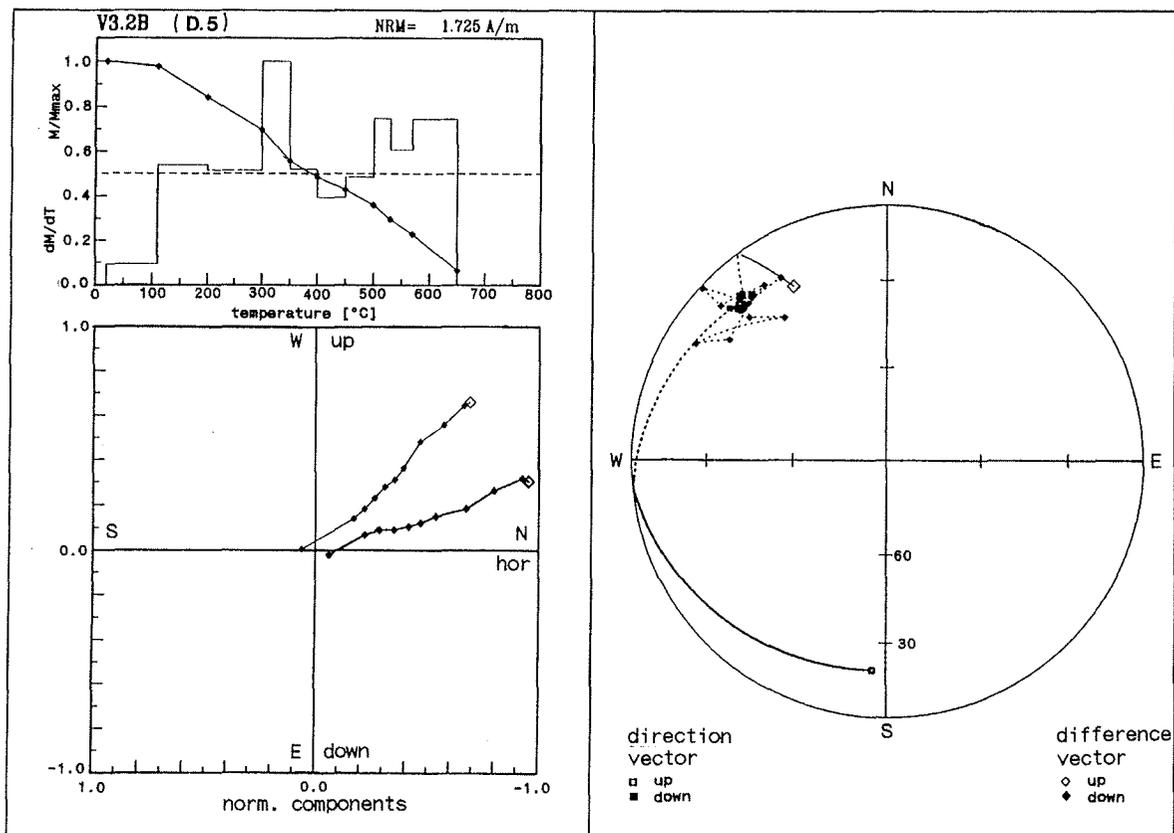

Fig. 17: Demagnetization behavior of the core samples of dyke 5. Top left = demagnetization curve (bold line, normalized with respect to the maximum magnetization) and the ratio of the change in magnetization to progressive change in temperature in each measuring interval (thin line); bottom left: Zijderveld diagram showing inclination (bold line) and delination (thin line); right = stereographic projection of the magnetic direction vectors (squares, bold lines) and difference vectors (rhombs, thin lines). The initial directions are marked by larger symbols. Dashed line: lower hemisphere; solid line: upper hemisphere.

Abb. 17: Entmagnetisierungsverhalten von Kernproben des Dyke 5. Links oben = Entmagnetisierungskurve (dicke Linie, normiert auf den Maximalwert) und Quotient aus Magnetisierungsänderung und progressiver Temperaturänderung in jedem Meßintervall (dünne Linie); links unten = Zijdervelddiagramm mit Darstellung der Inklination (dicke Linie) und Deklination (dünne Linie); rechts = Lagekugelprojektion der Richtungsvektoren (Quadrate, dicke Linien) und Differenzvektoren (Rauten, dünne Linien). Die Anfangsrichtungen sind durch größere Symbole gekennzeichnet. Gestrichelte Linie = untere Halbkugel; durchgezogene Linie = obere Halbkugel.
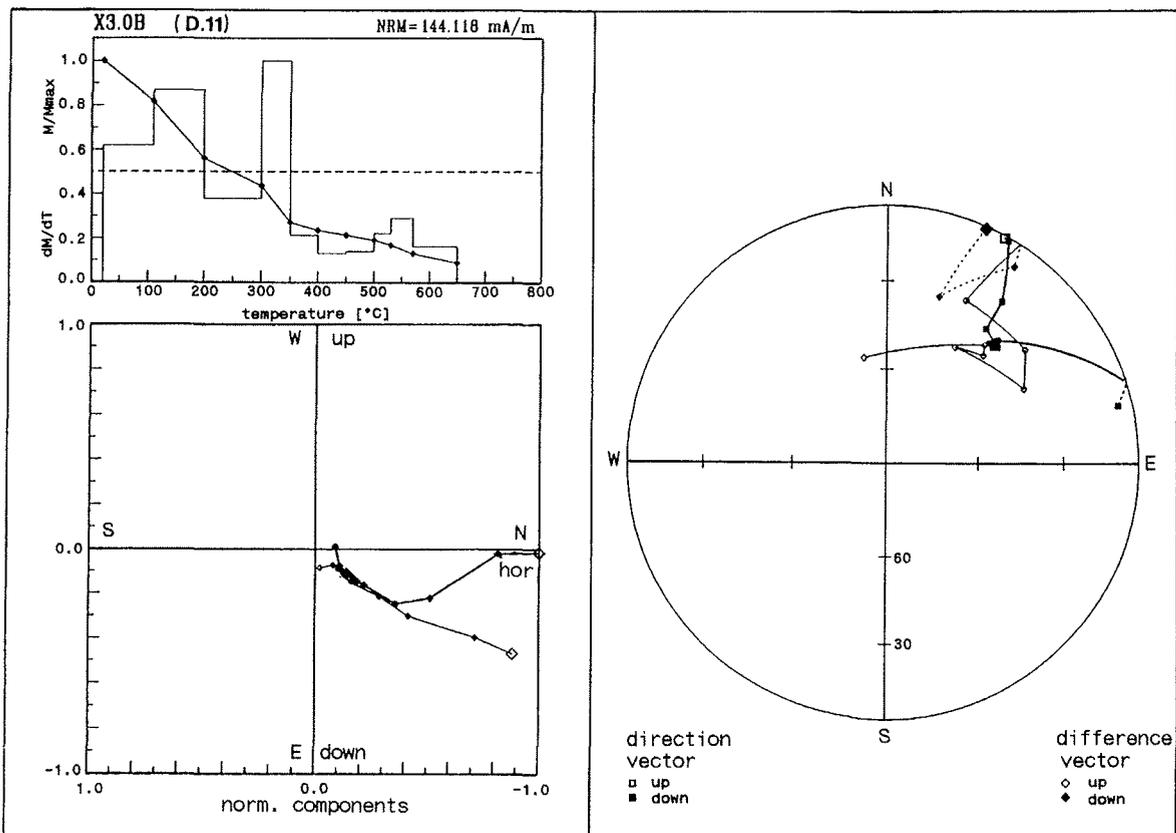
Fig. 18: Demagnetization behavior of the core samples of dyke 11. Top left = demagnetization curve (bold line, normalized with respect to the maximum magnetization) and the ratio of the change in magnetization to progressive change in temperature in each measuring interval (thin line); bottom left: Zijderveld diagram showing inclination (bold line) and delination (thin line); right = stereographic projection of the magnetic direction vectors (squares, bold lines) and difference vectors (rhombs, thin lines). The initial directions are marked by larger symbols. Dashed line: lower hemisphere; solid line: upper hemisphere.

Abb. 18: Entmagnetisierungsverhalten von Kernproben des Dyke 11. Links oben = Entmagnetisierungskurve (dicke Linie, normiert auf den Maximalwert) und Quotient aus Magnetisierungsänderung und progressiver Temperaturänderung in jedem Meßintervall (dünne Linie); links unten = Zijdervelddiagramm mit Darstellung der Inklination (dicke Linie) und Deklination (dünne Linie); rechts = Lagekugelprojektion der Richtungsvektoren (Quadrate, dicke Linien) und Differenzvektoren (Rauten, dünne Linien). Die Anfangsrichtungen sind durch größere Symbole gekennzeichnet. Gestrichelte Linie = untere Halbkugel; durchgezogene Linie = obere Halbkugel.

kind of behavior is shown by cores possessing a large proportion of secondary ore minerals formed by alteration of most of the primary titanomagnetite. It must be assumed that those directions with high blocking temperatures and showing similar declination and inclination values for other mineralogically similar cores represent CRMs imprinted at a later period.

Dyke 5 is an example of a dyke in which, in addition to a well-defined ChRM, another direction can be recognized in only a few of the cores. It has already been mentioned that secondary magnetite is the dominant carrier of the remanence. A stable direction with an inclination of about 33° occurs at temperatures above 350 °C (see Fig. 19).

In addition to secondary ore minerals, primary titanomagnetites are present displaying different stages of alteration. The cores with the second direction showing a very low inclination of -1° (Tab. 5) were probably collected from parts of the dyke with less magnetite, where the primary direction is preserved.

The cores from dyke 11 show similar results (Tab. 5). Two directions were also obtained for dyke 1; both have low inclinations and different pole positions to dykes 11 and 5.

The above examples represent not only two different types of demagnetization behavior but also the ChRM directions typical for the dykes of the Read Mountains. One of these directions has low inclination values (max. 14°) indicating a position near the equator when the remanent magnetization developed; declination values of these dykes are very variable (dykes 1, 2, 8, and 9, Tab. 5); the resulting pole positions are unlike any obtained for other dykes (Tab. 4).

The magnetization directions of other dykes (dykes 11a, 5a, and 6) are characterized by larger inclinations (up to about 43°) and declinations which produce relatively uniform pole positions (both normal and reverse orientations). They nearly correspond to the pole positions of the dykes of basalt group II from the northern and northwestern parts of the Shackleton Range (Tab. 4). The mean of these VGPs is 13.1 °S, 15.4 °E (k = 274; $\alpha_{95} = 7.5°$).
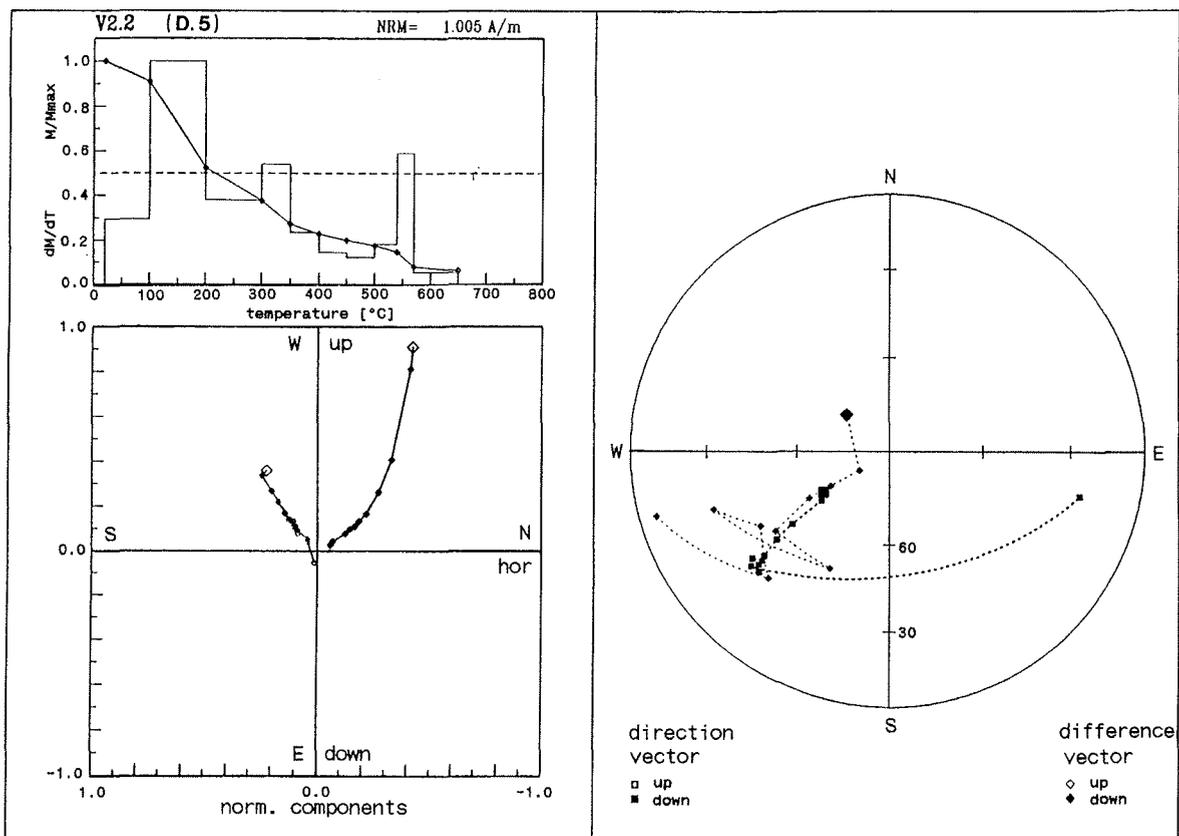
Fig. 19: Demagnetization behavior of the core samples of dyke 5. Top left = demagnetization curve (bold line, normalized with respect to the maximum magnetization) and the ratio of the change in magnetization to progressive change in temperature in each measuring interval (thin line); bottom left: Zijderveld diagram showing inclination (bold line) and delination (thin line); right = stereographic projection of the magnetic direction vectors (squares, bold lines) and difference vectors (rhombs, thin lines). The initial directions are marked by larger symbols. Dashed line: lower hemisphere; solid line: upper hemisphere.

Abb. 19: Entmagnetisierungsverhalten von Kernproben des Dyke 5. Links oben = Entmagnetisierungskurve (dicke Linie, normiert auf den Maximalwert) und Quotient aus Magnetisierungsänderung und progressiver Temperaturänderung in jedem Meßintervall (dünne Linie); links unten = Zijdervelddiagramm mit Darstellung der Inklination (dicke Linie) und Deklination (dünne Linie); rechts = Lagekugelprojektion der Richtungsvektoren (Quadrate, dicke Linien) und Differenzvektoren (Rauten, dünne Linien). Die Anfangsrichtungen sind durch größere Symbole gekennzeichnet. Gestrichelte Linie = untere Halbkugel; durchgezogene Linie = obere Halbkugel.

The magnetization directions on which this pole position is based are considered to be superimposed secondary, chemoremanent directions. They are obviously younger than the directions characterized by low inclinations. However, it is uncertain whether all other directions with low inclination correspond to the primary TRM or whether at least some of them are superimposed directions.

The characteristic remanent directions (ChRM) and the virtual geomagnetic pole positions (VGP) of the dykes in the Read Mountains are shown in Fig. 20. ChRM directions and VGPs that are the mean values of less than three rock samples or for which k values are less than 10 (Tab. 5) are in parentheses. The three superimposed CRM directions (larger inclinations) and the resulting VGPs of dykes 5, 6, and 11 are represented as rectangles.

4. CONCLUSIONS

The results of palaeomagnetic analysis led to conclusions about the age of the mafic dykes and the geotectonic status of the Shackleton Range.

4.1 *Importance of the results for determining the intrusion age*

Evidence of the age of the dykes can be obtained from isotope analyses (HOTTEN 1993, SPAETH et al. 1995) and of course from palaeomagnetic data, which gives the time when the remanent magnetization was acquired.

The virtual geomagnetic pole positions are interpreted individually below.

Two dyke samples in Group I (16a and b, not dyke 25) possess a TRM that can be determined precisely. The two resulting poles cannot be distinguished statistically, suggesting a similar age of intrusion. This is supported by radiometric age determinations

ChRM-directions

N

W

E

S

○ up
● down

VGPs
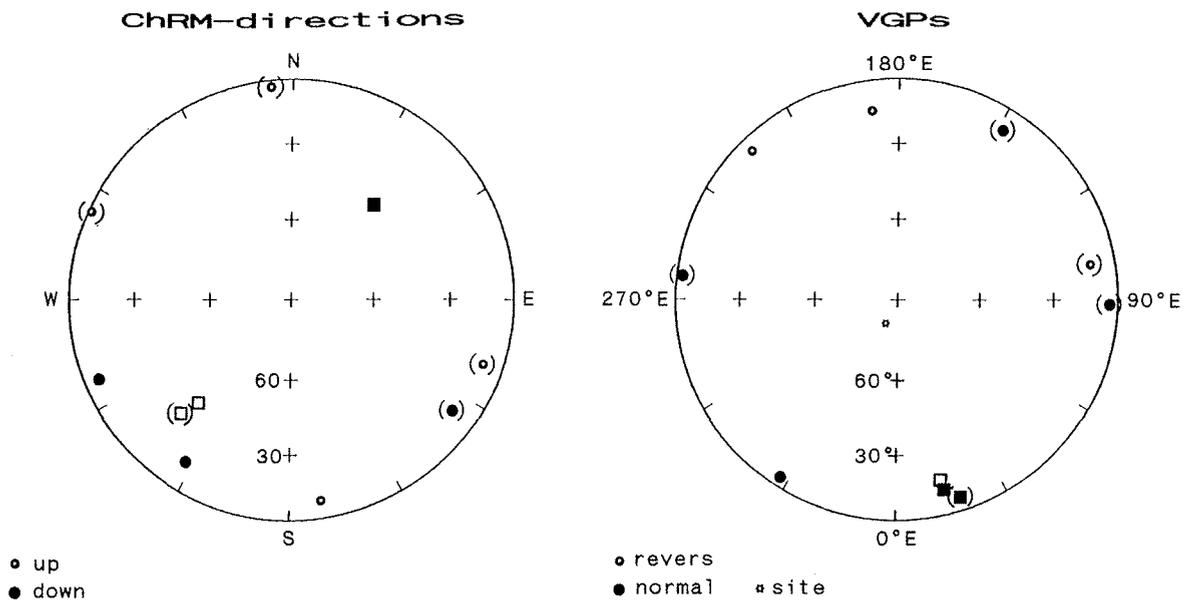
180°E

270°E

90°E

0°E

○ revers
● normal   ▪ site

Fig. 20: ChRM directions and VGPs for the dykes of Groups IV and V. Primary magnetization directions (left), and VGPs (right) calculated from them are represented as circles; the secondary (CRM) directions (left) and the VGPs (right) calculated from them are represented as squares. Directions and VGPs calculated from demagnetization data of less than two rock samples or for which k < 10 are shown in parentheses. ChRM directions are plotted on a Schmidt net; VGPs are plotted in a polar stereographic projection (lower hemisphere; projection plane = equator).

Abb. 20: ChRM-Richtungen und VGPs für Gänge der Gruppen IV und V. Als Kreis dargestellt sind primäre Magnetisierungsrichtungen und daraus errechnete VGPs, Quadrate stellen die sekundäre (CRM-)Richtungen und daraus ermittelte VGPs dar. Richtungen / VGPs, die aus Entmagnetisierungsdaten von weniger als zwei Gesteinsproben ermittelt wurden bzw. für die k < 10 ist, sind eingeklammert. Darstellung der ChRM-Richtungen im Schmidtschen Netz; Darstellung der VGPs in einer polständigen, flächentreuen stereographischen Projektion (untere Halbkugel; Projektionsebene: Äquatorebene)

and the field relationships, i.e. the two outcrops (16a and b) belong to the same dyke (HOTTEN 1993, SPAETH et al. 1995)). Since only two VGPs were determined and in this case non-dipole components and/or palaeosecular variations of the earth's magnetic field have not been eliminated, the calculated mean pole position is likely to deviate from the actual palaeomagnetic pole position.

It is more difficult to determine the primary magnetization directions of some dykes of basalt Group II than for those of Group I. ChRM directions and VGPs were determined for all six dykes (Tab. 4, Fig. 16) on the basis of stable magnetization directions and circles of remagnetization. The pole positions are again almost coincident and suggest that these dykes have similar ages.

The results of palaeomagnetic analysis of the dykes in the Read Mountains (Groups IV and V) are less reliable. The determination of stable directions is made more difficult or even impossible by hydrothermal alteration and low-grade regional metamorphism. The problems were described in the previous chapter. It should be borne in mind that the palaeomagnetic data on these dykes should be interpreted with care. The VGPs show a wide scatter; in contrast to the dykes of the northern and northwestern part of the Shackleton Range, the poles do not form a cluster, which might have suggested that a number of the dykes had a similar age.

K-Ar dating of the dykes of Group I give a Jurassic age (HOTTEN 1993; SPAETH et al. 1995). A mean VGP of 49.2 °S, 204.2 °E was obtained for the dykes of Mount Beney (Lagrange Nunataks; dykes 16a and b, Group I). It was not possible to determine the precision parameters k and α_{95} after FISCHER (1953), since there are only two VGPs.

Jurassic paleopole positions correspond with those of other regions in eastern Antarctica, e.g. the neighboring Theron Mountains and Whichaway Nunataks (Tab. 6 and Fig. 21). In particular PETERS (1989) obtained very similar pole positions (47.8 °S, 206.7 °E) for Jurassic basalts in Vestfjella (New Schwabenland). LIVERMORE et al. (1984) calculated a mean Jurassic pole for eastern Antarctica of 53.5 °S, 218.5 °E. The close correspondence between these pole positions confirms a Jurassic age of intrusion for the two Mount Beney dyke outcrops, which probably belong to a single dyke.

The other palaeomagnetically investigated dykes of the northern Haskard Highlands, the Lagrange Nunataks, and the Herbert Mountains (dykes of Group II) show different paleopole directions from those of the Jurassic dykes. Six VGPs obtained from the dykes of basalt Group II give a paleopole position of 30.8 °S, 1.9 °E (k = 18.2, α_{95} = 16.1°). Since the dykes of Group II cover a considerable range, this is value only represents an approximate pole position for an extended part of the Early Palaeozoic.

Plat (°S)	Plong (°E)	Locality / Author
49.2	204.2	Schackleton Range, Lagrange Nunataks, this paper
48	207	Neuschwabenland, Vestfjella, Peters 1989
42	226	Neuschwabenland, Vestfjella, Løvlie 1979
54	224	Theron Mountains, Whichaway Nunataks, Blundell 1966
49	227	Queen Alexandra Range, Ostrander 1971
58	218	Ferrar Glacier, Ferrar Dolerite, Tunrbull 1959
45	220	Wright- and Victoria Valley, Ferrar Dolerite, Bull et al. 1962
59	221	Bearmore Glacier, Ferrar Dolerite, Briden & Oliver 1963
56	202	Dufek Intrusion, Pensacola Mountains, Beck 1972
60	223	Forrestal Gabbro, Dufek Intrusion, Beck et al 1979
54	220	Transantarctic Mountains, Ferrar Dolerite, Irving 1964
71	226	Litell Rocks, Ferrar Supergroup, Delisle & Fromm 1984
55	222	David Glacier, Kirkpatrick Basalt, McIntosh et al. 1982
53	218	mean pole position for East Antarctica, Livermore et al. 1984

Tab. 6: Jurassic pole position of East Antarctica. P_{Lat}/P_{Long} = latitude/longitude of the poles.

Tab. 6: Jurassische Polpositionen Ostantarktikas. P_{Lat}/P_{Long} = geographische Breite/Länge der Pole.

LEGEND

▲ mean VGP of basalt Group I (2 values)
■ mean VGP of basalt Group II (6 values)
◆ mean VGP of the chemoremanent magnetized dykes of the Read Mountains, basalt Groups IV and V (3 values)

○ Jurassic paleopole positions of diverse regions in eastern Antarctica
△ mean jurassic paleopole positions of eastern Antarctica (LIVERMORE et al. 1984)
□ Middle Devonian paleopole positions of eastern Antarctica
◇ Cambrian-Ordovician paleopole positions of diverse regions in eastern Antarctica
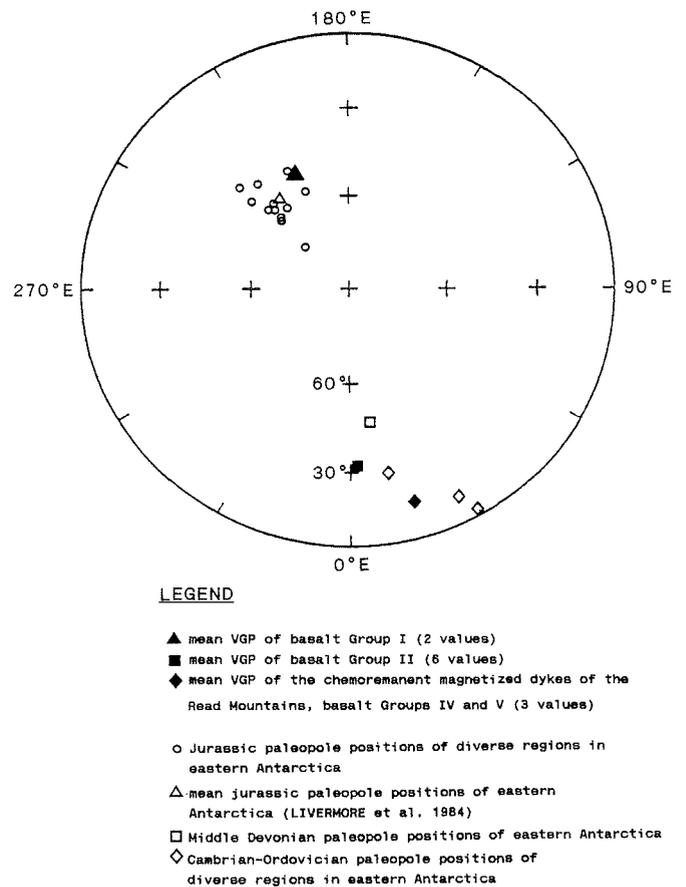
Fig. 21: Comparison of Jurassic, one Middle Devonian and Cambrian-Ordovician pole positions after several authors (see Tabs. 6 and 7), as well as the mean VGPs of the Shackleton Range dykes.

Abb. 21: Vergleich jurassischer, einer mitteldevonischen und kambrisch-ordovizischer Polpositionen nach verschiedenen Autoren (vgl. Tab. 6 und 7) mit den mittleren VGPs der Shackleton-Range-Gänge.

K-Ar age determinations on some dykes in the group II show Silurian-Devonian ages (HOTTEN 1993, SPAETH et al. 1995). Only three of the six dykes in this group (dykes 15, 24, and 27) were dated. The VGPs of all dykes in basalt Group II, which are nearly identical, indicate a Silurian-Devonian age for all the other dykes in this basalt group.

In Tab. 7, the mean VGPs obtained in this study are compared with similar pole postions from the literature, one Middle Devonian, three Lower Ordovician, and one Proterozoic. Fig. 21 shows the positions of the poles. The comparison shows that the mean VGP of the dykes in group II plots near those of the Palaeozoic poles from the literature mentioned in Tab. 7. The age of the remanent magnetization corresponds to the age of intrusion or cooling because the dykes of this basalt group are carriers of a primary thermoremanent magnetization. Some dy-

Plat (°S)	Plong (°E)	Locality	Age	Author
30.8	1.9	Northern Shackleton Range	Silurian-Devonian	this paper
13.1	15.4	Read Mountains, Shackleton Range	Ross event	this paper
47	8	Northern Victoria Land	Middle Devonian (361 ±5 Ma)	Delisle 1983
9	27	Taylor Valley, Victoria Land	Late Ordovician (470 Ma)	Manzoli & Nanni 1977
28	10	Sør Rondane Mountains, Queen Maud Land	Late Ordovician (480 Ma)	Zijderveld 1968
2	29	Mirny Station	Cambrian-Ordovician (502 Ma)	McQueen 1972
9	240	Ahlmannryggen, Neuschwabenland	Proterozoic (1100-1200 Ma?)	Peters 1989

Tab. 7: Palaeozoic and Proterozoic pole positions of East Antarctica. P_{Lat}/P_{Long} = latitude/longitude of the poles.

Tab. 7: Paläozoische und proterozoische Polpositionen Ostantarktikas. P_{Lat}/P_{Long} = geographische Breite/Länge der Pole.

kes in Group II give Silurian-Devonian K-Ar ages. The position of the mean VGP of the dykes in this group, which plots near the Cambrian-Ordovician and Middle Devonian poles from the literature, agrees closely with the K-Ar ages. In any case, comparison of the VGPs determined in this study with the data from the literature supports the Early Palaeozoic age of these dykes.

The distribution, K-Ar ages, and Sm-Nd model ages (HOTTEN 1993, SPAETH et al. 1995) all point to Proterozoic intrusion ages of the dykes in the Read Mountains.

Three of these dykes were found to be carriers of a secondary chemoremanent magnetization. No primary remanence can be determined. The ChRM directions and VGPs of the dykes are very similar, neglecting their different polarities, and the same age of acquisition of the remanence can be inferred (Fig. 20 and Tab. 5). The mean VGP of these three dykes of 13.1 °S, 15.4 °E (k = 274; α_{95} = 7.5°) corresponds more closely to the Cambrian-Ordovician paleopole positions of other regions in eastern Antarctica (Fig. 21 and Tab. 7) than to the mean VGP of the Early Palaeozoic dykes of basalt Group II (see above). The relevant event during which acquisition of the CRM probably took place was in Early Palaeozoic times, i.e. Cambrian or Ordovician.

The other VGPs of the Read Mountains dykes show a wide scatter and therefore cannot be assigned to any single event. However, the low angles of inclination giving pole positions near the equator are characteristic (Fig. 20 and Tab. 5). At the time the

remanence was acquired, the Shackleton Range area was near the equator. PETERS (1989) determined a Proterozoic pole position for the mafic dykes of New Schwabenland of 8.8 °S, 239.9 °E (α_{95} = 5.5°) (Tab. 7). A K-Ar age of 1100-1200 Ma was determined on biotite from these dykes.

Dyke 9 from the Read Mountains shows a VGP near this Proterozoic pole position (Tab. 5). It is possible that this dyke acquired its remanence contemporaneously with this VGP. However, judging by numerous slickensided fracture planes, dyke 9 is probably much faulted. This suggests that in this case, the only one) the close correspondence between the pole positions may be coincidental.

The pole positions obtained during this study were also compared with the apparent polar-wandering path (APWP) for the Gondwana Supercontinent covering the relevant periods.

THOMPSON & CLARK (1982) published an APWP for the Gondwana Supercontinent for the period between 550 and 160 Ma. It is based on a statistical interpretation of 219 reliable pole positions from the Gondwana continents which, on the basis of the Gondwana reconstruction of SMITH & HALLAM (1979), were rotated back relative to a fixed African continent.

The virtual geomagnetic pole positions (VGPs) described in this paper were also rotated using the model of SMITH & HALLAM (1970) (rotation of 58.4° around a Eulerian pole at 1.3 °N, 324 °E; reconstructed values for East Antarctica). In this way, the
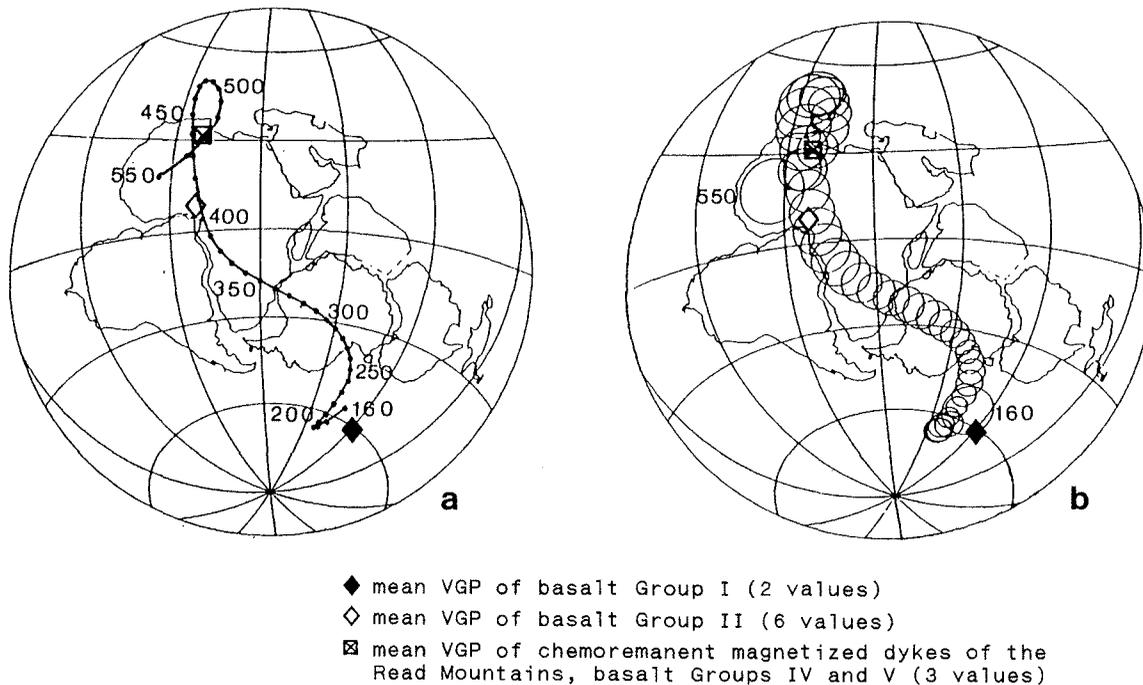

♦ mean VGP of basalt Group I (2 values)
◇ mean VGP of basalt Group II (6 values)
⊠ mean VGP of chemoremanent magnetized dykes of the
    Read Mountains, basalt Groups IV and V (3 values)

Fig. 22: Plot of APWP for Gondwana for the period from 550 to 160 Ma in 10 Ma intervals (a) with the appropriate α_{95} cones of confidence (THOMSON & CLARK 1982). The mean VGPs of the Shackleton Range rotated according to the Gondwana reconstruction model of SMITH & HALLAM (1976) are also shown.

Abb. 22: 550 bis 160 Ma-APWP für Gondwana in 10 Ma-Intervallen (a) und mit zugehörigen α_{95}-Vertrauensovalen (THOMSON & CLARK 1982). Hinzugefügt sind die nach dem Gondwana-Rekonstruktionsmodell von SMITH & HALLAM (1979) rotierten, mittleren VGPs der Shackleton Range.

information obtained so far about the less known paleopole positions of East Antarctica is supplemented by data from the Shackleton Range and can be compared with the Gondwana APWP. The VGPs described in this paper and the APWPs are shown in Fig. 22.

As was expected, the VGP of the Mount Beney basic dykes (basalt group I) plots near the Jurassic part of the path (rotated mean VGP at 62.0 °S, 97.3 °E). The deviation from the APWP can probably be explained by palaeosecular variation which was not eliminated because of the small number of VGPs (see 3.4). However, this supports an approximately Jurassic age.

The mean VGP of the six dykes of basalt Group II plots on the Palaeozoic part of the APWP and indicates an age of about 400-410 Ma (rotated mean VGP at 10.8 °N, 11.6 °E). The position of the mean VGP consequently corresponds with the K-Ar age of the dykes as Silurian to Devonian (HOTTEN 1993, SPAETH et al. 1995).

An additional mean VGP is derived from the chemoremanent magnetization of some dykes in the Read Mountains (dykes 5(a), 6, and 11(a), Tab. 5). This is a secondary magnetization and the corresponding VGP is identical with the earth's magnetic field at the time of its superimposition. Using SMITH & HALLAM's (1970) Gondwana model, this can also be correlated with the apparent polar-wandering path of THOMPSON & CLARK (1982) (rotated pole at 32.4 °N, 9.6 °E, Fig. 22). However, it is not possible to determine the age precisely because this part of the APWP forms a loop. But the age is older than that of the paleopole positions of the Northern Shackleton Range dykes. It correlates with the age of the Ross orogeny, which had its peak during the Cambrian and which, on account of the low metamorphic grade in the Read Mountains, was probably responsible for the secondary CRM in these rocks.

Additional Palaeozoic polar-wandering path for Gondwana have been published by BACHTADSE & BRIDEN (1990) and KENT & VAN DER VOO (1990). Both differ from the APWP of THOMPSON & CLARK (1982) in that the path turns back between the Late and/or Middle Silurian and the Early and/or Late Devonian. Comparison of the mean Palaeozoic VGPs for the Shackleton Range with the two APWPs shows reasonable correspondence with the Ordovician-Silurian part of the path. Differences from the APWP of BACHTADSE & BRIDEN (1990) result from their use of LAWVER & SCOTESE's (1987) Gondwana reconstruction. As a result, the paleopoles of West Gondwana are about 150 west of SMITH & HALLAM's (1970) reconstruction; the polar-wandering path is shifted correspondingly. Nevertheless, comparisons with these APWPs confirm the magnetization age of the dykes of Group II and the age of the chemoremanent magnetization of the Read Mountains dykes as Early Palaeozoic.

A Proterozoic apparent polar-wandering path for the southern part of Africa was determined by McWILLIAMS & KRÖNER (1981). Using the same Gondwana reconstruction method as used for the dykes of the northern and northwestern parts of the Shackleton Range (see above), the VGPs of the Read Mountains

were rotated relative to Africa and are compared with the Proterozoic APWP.

The following rotated pole positions are based on the palaeomagnetically determined poles are given in Tab. 5.

Dyke		
1(a)	9.9 °N	318.0 °E
1(b)	48.8 °S	284.9 °E
5	45.4 °N	336.1 °E
5(b)	40.7 °S	284.5 °E
8	6.2 °N	322.9 °E
9	63.9 °N	34.3 °E
11	27.5 °S	288.4 °E

Comparison of these with the Proterozoic APWP (McWILLIAMS & KRÖNER 1981) mentioned above is problematic for several reasons. Firstly, the APWP is based on unreliable data. The APWP was calculated on the basis of palaeomagnetic data from the Congo and Kalahari cratons (southern Africa). This method is only applicable if no relative movement took place between these two cratons during the entire investigated period. This situation would fit McWILLIAMS & KRÖNER's (1981) model, but contrasts with the ideas of BURKE et al. (1976), which imply that the Pan-African geotectonics are collisional. It is clear that no major movements took place here, as paleopole positions on the two cratons were determined for this period as well as for the time of the Pan-African orogeny and they correspond reasonably closely.

Those VGPs determined in this study that plot near the equator are subject to an additional uncertainty (Fig. 20). The relatively large statistical error in the ChRM directions and the corresponding pole positions (Tab. 5) do not permit the north and south poles to be distinguished. It is therefore uncertain which pole position should be compared with the apparent polar-wandering path based on south pole positions.

Additionally, any comparison with the Proterozoic polar-wandering path for South Africa is only possible if it can be assumed that West and East Gondwana were connected during the relevant period. On the basis of palaeomagnetic analysis of rocks from different regions of West and East Gondwana, several authors (McWILLIAMS1981, DALZIELL 1991, KRÖNER 1991) postulate that these two regions were separate continents; DALZIEL (1991) postulated the existence of a so-called „Mozambique Ocean" between East and West Gondwana, which is postulated as not having closed before the end of the Late Proterozoic. McWILLIAMS (1981) also refers to the uncertainties of interpreting palaeomagnetic data from Proterozoic rocks, e.g. the very small amount of data, uncertain magnetization ages and uncertainties due to tectonic deformation. Contradictory interpretations of Proterozoic Gondwana show that the pre-Palaeozoic history of the continent or discrete parts of it is insufficiently known.

Therefore, the comparative interpretation of the possible Proterozoic VGPs is uncertain. Dyke 5, which gives a biotite age

of 1250-1350 Ma (see above), can be assigned to a section of the APWP of comparable age (McWilliams & Kröner, 1981, (Fig. 23). Dyke 9, which has an age of 823 ± 67 Ma after Paech (pers. comm.), plots on the path at 1.2 Ma. Since this dyke has probably suffered some deformation (epidote slickensides on joint surfaces), the VGP may not be entirely reliable.

It is noteworthy that all VGPs plot on or near this APWP (Fig. 23). In addition to the results of the previous investigation of the age of the Read Mountains dykes, this is further evidence for a Middle to Late Proterozoic age of the dykes. However, it is not possible to obtain more detailed information from the palaeomagnetic data in this case.
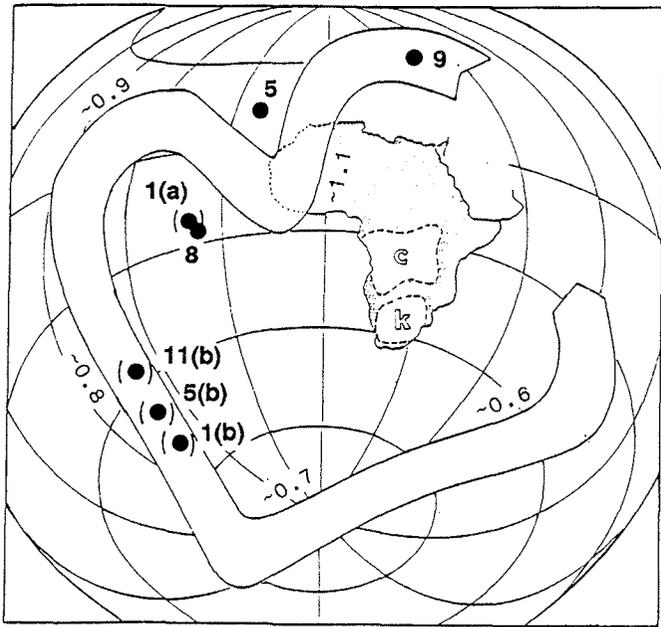

Fig. 23: Plot of APWP for the Congo (c) and Kalahari (k) cratons for the period from 1.2 to 0.6 Ga (McWilliams & Kröner 1981). The dots represent the VGPs of the Read Mountains dykes rotated according to the Gondwana reconstruction model of Smith & Hallam (1976).

Abb. 23: 1,2 bis 0,6 Ga-APWP für den Congo- (c) und den Kalahari- (k) Kraton, südliches Afrika (McWilliams & Kröner 1981). Die Punkte repräsentieren die nach dem Gondwana-Rekonstruktionsmodell von Smith & Hallam (1979) rotierten VGPs der Read-Mountains-Gänge.

4.2 The significance of the results with respect to the geotectonic setting of the Shackleton Range

The difference between the main trend of the Shackleton Range (E-W) and that of the Ross Orogen (N-S to NE-SW) has given rise to different ideas concerning its allochthonous or autochthonous nature. The possibility is discussed in the literature whether the Shackleton Range crustal block rotated and drifted to its present position from its original position parallel to the western margin of the East Antarctic Shield or parallel to the main trend of the Ross Orogen. This rotation could have been caused by the break-up of the Gondwana supercontinent. This would have been similar to that postulated for the Ellsworth Mountains block (Schopf 1969). Several authors infer an au-

tochthonous origin for the Shackleton Range, i.e. the product of an upfolded aulacogen or an orogen above a subduction zone (Hofmann & Paech 1980, Kamenev & Semenov 1980, Clarkson 1982, Marsh 1983, Pankhurst et al. 1983, Buggisch et al. 1990). If the Shackleton Range is an aulacogen, then the true Ross Orogen must be further west (Hofmann & Weber 1983, Spaeth & Fielitz 1991).

The palaeomagnetic data in this paper can contribute towards resolving these geotectonic problems. The Mesozoic and Palaeozoic pole positions of Shackleton Range rocks correspond with pole positions of the same age for other East Antarctic areas, particularly with that for the Jurassic basalt at Vestfjella, New Schwabenland, determined by Peters(1989), and with the well-documented polar-wandering path for Gondwana (Thompson & Clark 1982); this indicates that the Shackleton Range is authochthonous and makes it improbable that significant rotation or shifting of the crustal block has taken place.

Various rotations of the Shackleton Range were simulated mathematically with the purpose of testing which pole positions are generated from the palaeomagnetic data assuming another orientation of the Shackleton Range. This should test whether there is any concordance between the mean VGPs and Thompson & Clark's (1982) polar-wandering path for Gondwana, e.g. if the poles are shifted parallel to the polar-wandering path. For this purpose, the mean VGPs were rotated clockwise and anticlockwise around a point at 80.5 °S, 334.0 °E (approximately the centre of the Shackleton Range) in steps of 5° and then compared with the Palaeozoic-Mesozoic APWP for Gondwana using the Smith & Hallam (1970) reconstruction model. The resulting curve of the VGPs is shown in Fig. 24 up to an angle of rotation of 145°.

This diagram shows that rotation causes the calculated pole positions for the Shackleton Range to move rapidly away from the apparent polar-wandering path. Thus, if the Shackleton Range had had another position at the time of magnetization of the dykes (which means at the time of intrusion and cooling of the Mesozoic and Palaeozoic dykes and/or superimposition of a chemoremanent magnetization on the Proterozoic dykes), then its position would not correspond with the APWP.

Similarly, considerable rotation of the crustal block into its present position must also be rejected. These results strongly suggest that the Shackleton Range is autochthonous in its present position.

It is now possible, on this basis, to make a supraregional comparison of the extensional movements, the directions of which can be deduced from the directions of the dykes of different ages. Dykes in the Pensacola Mountains, the Shackleton Range, and western New Schwabenland were intruded during the late Proterozoic and Jurassic in the same, or similar, N-S to NE-SW directions (Ford et al. 1978, Schmidt et al. 1978, Peters et al. 1986, Spaeth & Fielitz 1987, Spaeth & Schüll 1987, Peters 1989). This behavior indicates that during these two periods the crust in the wider area of the Ross Orogen was sub-
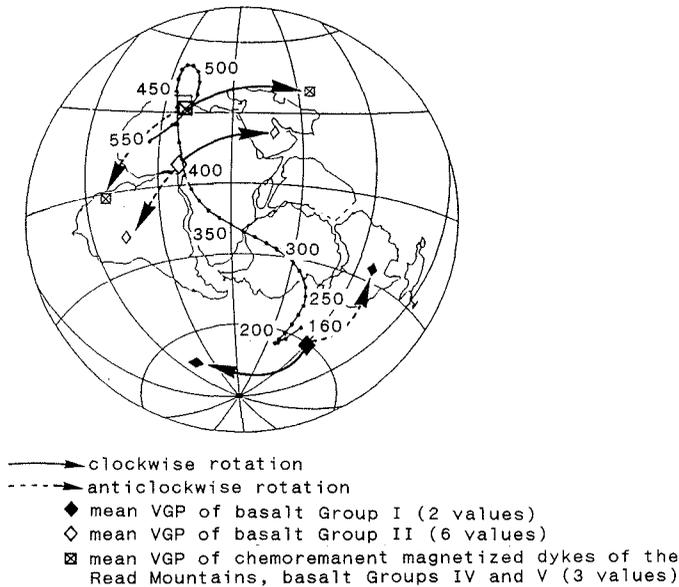
── clockwise rotation
---- anticlockwise rotation
◆ mean VGP of basalt Group I (2 values)
◇ mean VGP of basalt Group II (6 values)
⊠ mean VGP of chemoremanent magnetized dykes of the
    Read Mountains, basalt Groups IV and V (3 values)

Fig. 24: Mean VGPs of the Shackleton Range with representation of the Gondwana APWP after THOMSON & CLARK (1982). The Shackleton Range was rotated clockwise and counterclockwise up to an angle of 45°; the resulting „paths" of the VGPs are represented by arrows.

Abb. 24: Mittlere VGPs der Shackleton Range mit Darstellung der Gondwana-APWP nach THOMSON & CLARK (1982). Die Shackleton Range wurde im und entgegen dem Uhrzeigersinn bis zu einem Winkel von 45° rotiert; die daraus resultierenden „Bewegungsbahnen" der VGPs sind durch Pfeile dargestellt.

ject to extension in a common stress field; they were not local stresses but affected a large area of East Antarctica and, at least during the Jurassic (SPAETH & SCHÜLL 1987), large parts of Gondwana. The two phases of extensional tectonics documented in the Shackleton Range by the intrusion of mafic dykes between two orogenic cycles, firstly during the Proterozoic and secondly, during the Palaeozoic and Jurassic periods, are compatible with an autochthonous Shackleton Range within the tectonic framework of Gondwana.

ACKNOWLEDGEMENTS

References

Ade-Hall, J.M., Khan, M.A., Dagley, P. & Wilson, R.L. (1968): A Detailed opaque petrological and magnetic investigation of a single Tertiary lava from Skye, Scotland. Part I and II.- Geophys. J. 16: 374-399.

Ade-Hall, J.M., Palmer, H.C. & Hubbard, T.P. (1971): The magnetic and opaque petrological response of basalts to regional hydrothermal alteration.- Geophys. J. R. Astr. Soc. 24: 137-174.

Bachtadse, V. & Briden, J.C. (1990): Palaeomagnetic constraints on the position of Gondwana during Ordovician to Devonian times. - In: W.S. McKERROW & C.R. SCOTESE (eds), Palaeozoic Palaeogeography and Biogeography, Geol. Soc. Mem. 12: 43-48.

Beck, M.E. (1972): Palaeomagnetism and magnetic polarity zones in the Jurassic Dufek Intrusion, Pensacola Mountains, Antarctica.- Geophys. J. R. Astr. Soc. 28: 49-63.

Beck, M.E., Burmester, R.F. & Sheriff, S.D. (1979): Field reversal and paleomagnetic pole for Jurassic Antarctica.- EOS, Transactions Amer. Geophys. Union 60: 818.

Blundell, D.J. (1966): Palaeomagnetism of the dolerite intrusions, pt. 4, in Geology-(pt).1, Theron Mountains, Shackleton Range and Whichaway Nunataks.- Scientific Reports, Trans-Antarctic-Expedition 1955-1958, 8: 61-67, London.

Böhnel, H. (1985): Paläomagnetische Untersuchungen an jurassischen bis quartären Gesteinen aus Zentral- und Südmexiko.- Dissertation, Inst. Geophys. Univ. Münster, 234 S.

Briden, J.C. & Oliver, R.L. (1963): Paleomagnetic results from the Beardmore Glacier region, Antarctica.- N.Z. J. Geol. Geophys. 6: 388-394.

Buggisch, W., Kleinschmidt, G., Kreizer, H. & Krumm, S. (1990): Stratigraphy, metamorphism and nappe-tectonics in the Shackleton Range (Antarctica).- Geod. Geoph. Veröff. R.1 H.15: 64-86; Berlin.

Bull, C., Irving, E. & Willis, I. (1962): Further paleomagnetic results from South Victoria Land, Antarctica.- Geophys. J. R. Astr. Soc. 6: 320-336, London.

Burke, K.C.A., Dewey, J.F. & Kidd, W.S.F. (1976): Precambrian paleomagnetic results compatible with contemporary operation of the Wilson Cycle.- Tectonophysics 33: 287-299.

Clarkson, P.D. (1982): Tectonic significance of the Shackleton Range.- In: C. Craddock (ed.), Antarctic Geoscience: 835-839, Univ. Wisconsin Press, Madison.

Dalziel, I.W.D. (1991): Pacific margins of Laurentia and East Antarctica-Australia as a conjugate rift pair: evidence and implications for an Eocambrian supercontinent.- Geology 19: 598-601.

Delisle, G. (1983): Results of paleomagnetic investigations in Northern Victoria Land, Antarctica.- In: R.L. OLIVER, P.R. JAMES & J.B. JAGO (eds), Antarctic Earth Science, Proc. 4th Int. Symp. on Antarctic Earth Sciences, 146-149, Canberra.

Delisle, G. & Fromm, K. (1984): Paleomagnetic investigation of Ferrar Supergroup rocks, North Victoria Land, Antarctica.- Geol. Jb. B60: 41-55, Hannover.

Doell, R.R. & Cox, A. (1965): Palaeomagnetism on Hawaii.- J. Geophys. Res. 70: 3377.

Dunlop, D.J. (1981): The rock magnetism of fine particles.- Phys. Earth Planet. Internat. 26: 1-26, Amsterdam.

Fisher, R.A. (1953): Dispersion on a sphere.- Proc. R. Soc. Astr. 217: 295-305, London.

Ford, A.B., Schmidt, D.L. & Boyd (jr.), W.W. (1978): Geologic map of the Davis Valley quadrangle and part of the Cordiner Peaks quadrangle, Pensacola Mountains, Antarctica.- U.S. Antarctic Res. Program Map, U.S. Geological Survey.

Halls, H.C. (1976): A least squares method to find a remanence direction from converging remagnetisation circles.- Geophys. J. R. Astr. Soc. 45: 297-304.

Halls, H.C. (1978): The use of converging remagnetisation circles in palaeomagnetism.- Phys. Earth Planet. Int. 16: 1-11, Amsterdam.

Hargraves, R.B. & Petersen, N. (1971): Notes on the correlation between petrology and magnetic properties of basaltic rocks.- Z. Geophysik 37: 367-382.

Hofmann, J. & Paech, H.J. (1980): Zum strukturgeologischen Bau am Westrand der Ostantarktischen Tafel.- Z. geol. Wiss. 8: 425-437, Berlin.

Hofmann, J. & Weber, W. (1983): A Gondwana reconstruction between Antarctica and South Africa.- In: R.L. OLIVER, P.R. JAMES & J.B. JAGO (eds), Antarctic Earth Science: 584-589, Canberra.

Hotten, R. (1993): Die mafischen Gänge der Shackleton Range/Antarktika: Petrographie, Geochemie, Isotopengeochemie und Paläomagnetik.- Berichte Polarforschung 118, 1-225.

Irving, E. (1964): Paleomagnetism and Its Application to Geological and Geophysical Problems.- 399 S., John Wiley and Sons Inc., New York.

Johnson, H.P. & Hall, J.M. (1978): A detailed rock magnetic and opaque mineralogy study of the basalts from the Nazca Plate.- Geophys. J. 52: 45-64.

Kamenev, E.N. & Semenov, V.S. (1980): Regional metamorphism in Antarctica.- In: M.M CRESSWELL & P. VELLA (eds.), Gondwana Five, 209-215, A.A. Balkema, Rotterdam.

Kent, D.V. & Van der Voo, R. (1990): Palaeozoic palaeogeography from palaeomagnetism of the Atlantic-bordering continents.- In: W.S. McKERROW & C.R. SCOTESE (eds), Palaeozoic Palaeogeography and Biogeography, Geol. Soc. Mem. 12: 49-56.

Khramov, A.N. (1958): Palaeomagnetism and stratigraphic correlation.- In: E. IRVING, Paleomagnetism and Its Application to Geological and Geophysical Problems, Whiley, New York, N.Y., 1964, p. 75.

Kröner, A. (1991): African linkage of Precambrian Sri Lanka.- Geol. Rundschau 80: 429-440.

Lawver, L.A. & Scotese, C.R. (1987): A revised reconstruction of Gondwanaland.- In: McKENZIE, G.D. (ed.), Gondwana Six: Structure, Tectonics and Geophysics, Amer. Geophys. Union, Monogr. 40: 17-23.

Livermore, R.A., Vine, F.J. & Smith, A.G. (1984): Plate motions and the geomagnetic field - II. Jurassic to Tertiary.- Geophys. J. R. Astr. Soc. 79: 939-961.

Løvlie, R. (1979): Mesozoic palaeomagnetism in Vestfjella, Dronning Maud Land, East Antarctica.- Geophys. J. R. Astr. Soc. 59: 529-537.

Løvlie R. (1987): Evidence for deuteric magnetization in hydrothermally altered Mesozoic basaltic rocks from East Antarctica.- Physics Earth and Planetary Interiors 52: 352-364, Amsterdam.

Manzoni, M. & Nanni, T. (1977): Palaeomagnetism of Ordovician lamprophyres from Taylor Valley, Victoria Land, Antarctica.- Pure Appl. Geophys. 115: 961-977.

Marsh, P.D. (1983): The Late Precambrian and Early Palaeozoic history of the Shackleton Range, Coats Land.- In: R.L. OLIVER, P.R. JAMES & J.H. JAGO (eds.), Antarctic Earth Science, 190-193, Canberra.

McIntosh, W.C., Kyle, P.R., Cherry, E.M. & Noltimer, H.C. (1982): Paleomagnetic results from the Kirkpatrick Basalt Group, Victoria Land.- Antarctic J. US 17/4: 20-22, Washington.

McQueen, D.M., Scharnberger, L., Scharon, L. & Halpern, M. (1972): Cambro-Ordovician palaeomagnetic pole position and rubidium-strontium total rock isochron for charnockitic rocks from Mirny Station, East Antarctica.- Earth Planet. Sci. Lett. 16: 433-438, Amsterdam.

McWilliams, M.O. (1981): Palaeomagnetism and Precambrian tectonic evolution of Gondwana.- In: A. KRÖNER (ed.), Developments in Precambrian Geology 4, Precambrian Plate Tectonics, 648-687, Elsevier, Amsterdam.

McWilliams, M.O. & Kröner, A. (1981): Paleomagnetism and tectonic evolution of the Pan-African Damara Belt, Southern Africa.- J. Geophys. Res. 86: 5147-5162.

Ostrander, J.H. (1971): Paleomagnetic investigations of the Queen Victoria Range, Antarctica.- Ant. J. US 6(S): 183-185, Washington.

Pankhurst, R.J., Marsh, P.D. & Clarkson, P.D. (1983): A geochronological investigation of the Shackleton Range.- In: R.L. OLIVER, P.R. JAMES & J.B. JAGO (eds.), Antarctic Earth Science, 176-182, Canberra.

Peters, M. (1989): Die Vulkanite im westlichen und mittleren Neuschwabenland, Vestfjella und Ahlmannryggen, Antarktika. Petrographie, Geochemie, Geochronologie, Palaomagnetismus, geotektonische Implikationen.- Berichte Polarforsch. 61: 1-186 S.

Peters, M., Behr, H.J., Emmermann, R., Kohnen, H. & Weber, K. (1986): Alter und geodynamische Stellung der Vulkanitserien im westlichen Neuschwabenland (Antarktika).- Nachr. Dt. Geol. Ges. 35: 64-65.

Petersen, N. (1982): Gesteinsmagnetismus. - Unveröffentl. Manuskr., Inst. Allg. Angew. Geophys. Univ. München, 71 S.

Price, G.D. (1980): Exolution microstructures in titano magnetites.- Phys. Earth Planet. Int. 23: 2, Amsterdam.

Schmidbauer, E. (1975): Magnetic hysteresis loops and magnetisation versus temperature curves of some basalt samples containing titanomagnetite ore either single-phase or with an intergrowth of ilmenite lamellae.- J. Geophys. 41: 615-632.

Schmidt, D.L., Williams, P.L. & Nelson, W.H. (1978): Geologic map of the Schmidt Hills quadrangle and part of the Gambacorta Peak quadrangle, Pensacola Mountains, Antarctica.- US Geol. Survey Antarctic Geol. Map A-8, scale 1: 250 000.

Schopf, J.M. (1969): Ellsworth Mountains: position of West Antarctica due to sea floor spreading.- Science 164: 63-66.

Smith, A.G. & Hallam, A. (1970): The fit of the southern Continents.- Nature 225: 139-144.

Spaeth, G. & Fielitz, W. (1987): Structural investigations in the Precambrian of western Neuschwabenland, Antarctica.- Polarforschung 57: 71-92.

Spaeth, G. & Fielitz, W. (1991): Structural evolution of western Neuschwabenland and the Shackleton Range - a comparision.- In: H. ULBRICH & A.C. ROCHA CAMPOS (eds.), Gondwana Seven Proceedings, Sao Paulo.

Spaeth, G., Hotten, R., Peters, M. & Techmer, K. (1995): Mafic dykes in the Shackleton Range, Antarktica.- Polarforschung 63: 101-121.

Spaeth, G. & Schüll, P. (1987): A survey of Mesozoic dolerite dikes from western Neuschwabenland, Antarctica, and their geotectonic significance.- Polarforschung 57: 93-113.

Stacey, F.D. & Banerjee, S.K. (1974): The Physical Principles of Rock-Magnetism.- Elsevier, Amsterdam.

Thompson, R. & Clark, R.M. (1982): A robust least-squares Gondwanan apparent polar wander path and the question of palaeomagnetic assessment of Gondwanan reconstructions.- Earth Planet. Sci. Let. 57: 152-158.

Thompson, R. & Oldfield, F. (1986): Environmental Magnetism.- Allen & Unwin (Publishers) Ltd, London.

Turnbull, G. (1959): Some palaeomagnetic measurements in Antarctica.- Arctic 12: 151-157, Montreal.

Wilson, R.W. & Watkins, N.D. (1967): Correlation of petrology and natural magnetic polarity in Columbia Plateau basalts.- Geophys. J. R. Astr. Soc. 12: 405-424.

Worm, H.-U. (1981): Experimentelle Untersuchungen thermomagnetischer Eigenschaften von magmatischen Gesteinen.- Unveröffentl. Dipl.-Arbeit, Inst. Geophys. Univ. Bochum, 153 S.

Zijderveld, J.D.A. (1968): Natural remanent magnetisations of some intrusive rocks form the Sør Rondane Mountains, Queen Maud Land, Antarctica.- J. Geophys. Res. 73: 3773-3785.